Programmed “disarming” of the neutrophil proteome reduces the magnitude of inflammation

Jose M. Adrover[1], Alejandra Aroca-Crevillén[1], Georgiana Crainiciuc[1], Fernando Ostos[2], Yeny Rojas-Vega[3], Andrea Rubio-Ponce[1], Catia Cilloniz[4], Elena Bonzón-Kulichenko[5], Enrique Calvo[5], Daniel Rico[6], María A. Moro[2], Christian Weber[7,8], Ignacio Lizasoaín[2], Antoni Torres[4], Jesús Ruiz-Cabello[3,9], Jesús Vázquez[5] and Andrés Hidalgo[1,7]

[1] Area of Cell and Developmental Biology, Fundación Centro Nacional de Investigaciones Cardiovasculares, 28029 Madrid, Spain
[2] Unidad de Investigación Neurovascular, Department of Pharmacology, Faculty of Medicine, Universidad Complutense and Instituto de Investigación Hospital 12 de Octubre (i+12), Madrid, Spain
[3] Advanced Imaging Unit, Fundación Centro Nacional de Investigaciones Cardiovasculares, 28029 Madrid, Spain
[4] Department of Pneumology, Institut Clinic de Respiratori, Hospital Clinic of Barcelona, and Institut d’Investigacions Biomèdiques August Pi i Sunyer (IDIBAPS), University of Barcelona, Ciber de Enfermedades, Barcelona, Spain
[5] Cardiovascular Proteomics Laboratory, Centro Nacional de Investigaciones Cardiovasculares Carlos III (CNIC), Madrid, Spain; and Centro de Investigación Biomédica en Red de Enfermedades Cardiovasculares (CIBERCV), Madrid, Spain
[6] Institute of Cellular Medicine, Newcastle University, Framlington Place, Newcastle upon Tyne NE2 4HH, UK
[7] Institute for Cardiovascular Prevention, Ludwig Maximillians University, Munich, Germany
[8] German Cardiovascular Research Centre (DZHK), partner site Munich Heart Alliance, Munich, Germany and Dept. Biochemistry, Cardiovascular Research Institute Maastricht (CARIM), Maastricht, The Netherlands.
[9] CIC biomaGUNE, 2014, Donostia-San Sebastián, Spain; IKERBASQUE, Basque Foundation for Science, Spain; Ciber de Enfermedades Respiratorias (CIBERES), Madrid, Spain; and Universidad Complutense Madrid, Madrid, Spain.

Correspondence: Andres Hidalgo (ahidalgo@cnic.es)

Abstract

The anti-microbial functions of neutrophils are facilitated by a defensive armamentarium of proteins stored in granules, and by the formation of neutrophil extracellular traps (NETs). However, the toxic nature of these structures poses a threat to highly vascularized tissues, such as the lungs. Here, we identified a cell-intrinsic program that modified the neutrophil proteome in the circulation and caused the progressive loss of granule content and the reduction of the NET-forming capacity. This program was driven by the receptor CXCR2 and by regulators of circadian cycles. As a consequence, lungs were protected from inflammatory injury at times of day or in mouse mutants in which granule content was low. Changes in the proteome, granule content and NET formation also occurred in human neutrophils, and correlated with the incidence and severity of respiratory distress in pneumonia patients. Our findings unveil a "disarming" strategy of neutrophils that depletes protein stores to reduce the magnitude of inflammation.

Neutrophils are endowed with highly specialized features to combat infections. They accumulate receptors, proteases, antimicrobial peptides and proteins inside cytoplasmic granules that mediate the production of reactive oxygen species (ROS) or DNA-based extracellular traps (NETs), both of which are highly toxic and allow for effective containment of pathogens [1, 2]. Several types of granules coexist in the neutrophil cytoplasm [3], including primary (azurophilic) granules that store myeloperoxidase (MPO), secondary (specific) and tertiary (gelatinase) granules and secretory vesicles, each of which carries distinct types of cargo [1, 4]. The different granules form at different stages of granulopoiesis in the bone marrow [5, 6], and the synthesis of granule proteins declines as neutrophils differentiate [7, 8]. In contrast, receptors needed for sensing, migration and phagocytosis are mostly synthesized once they reach the circulation [7, 8].

After only 6-10 hours in the circulation [9], neutrophils rapidly disappear from blood [10, 11]. However, this does not imply immediate elimination, as they can be found within the vessels or parenchyma of multiple organs, with a preference for the spleen, bone marrow and lungs [10]. The homeostatic infiltration of granule-laden neutrophils, a process enabled by a cell-intrinsic program that relies on the chemokine receptor CXCR2 and the core clock protein Bmal1[12], can be potentially damaging to highly vascularized tissues such as the lungs. Indeed, lungs are highly susceptible to neutrophil-mediated damage that can cause respiratory dysfunction and death, as shown in murine models of lung injury [13, 14, 15]. In humans, neutrophil-mediated acute vascular damage followed by pulmonary edema and distress is common in patients with underlying pneumococcal infections or other pre-existing conditions [13, 16].

Here we investigated whether specific mechanisms prevent neutrophil-inflicted toxicity in tissues. We discovered that the neutrophil proteome spontaneously “disarms” as they lose granule content during their lifetime in circulation. This resulted in a blunted capacity to produce NETs, rendering the neutrophils less toxic before they reached tissues and protected the lungs from injury both in mice and in pneumonia patients.

Results

The neutrophil proteome changes during the day

Neutrophils undergo transcriptional changes while in the circulation [12]. However, because transcriptional changes take relatively long time (in the range of hours) and diurnal transcriptional programs in mouse neutrophils favor their migration into tissues, we deemed transcriptional regulation insufficient to protect the tissues from the toxic activity of neutrophils.

We undertook a proteomic approach to explore the changes in protein content in neutrophils at different times after release from the bone marrow. Because the number of neutrophils that can be purified from the blood of naïve mice at night (when neutrophils are released from the bone marrow) or at noon (when neutrophils have spent several hours in the circulation)[17] is low, we increased the number of night-like neutrophils released from the bone marrow by a one-time intraperitoneal injection at zeitgeber time 4 (ZT4, or 4 hours after lights on) of AMD3100, an antagonist for CXCR4 that induces the rapid mobilization of neutrophils from the bone marrow [18]. To increase the number of day-like neutrophils in circulation we injected blocking antibodies against endothelial selectins (1mg/kg, intravenously at ZT5 at days -5, -3 and -1 before collection)[12, 17] (**Extended Data Fig. 1a**). The proteomic analysis of these night- and day-like neutrophils isolated at ZT5 from the blood of wild-type mice yielded 6677 proteins (**Supplementary Table 1**). 171 proteins were differentially detected in one versus the other group, with proteins involved in regulation of the cytoskeleton (Arghdib, Rufy3), adhesion (Thbs1, Itgam), inflammasome (Nlrp3, Nlrp4e) and vesicular transport (Vps33b; **Fig. 1a**) enriched in night-like neutrophils. The differential expression of identified proteins in night- versus day-like neutrophils, such as VEGFR1, CD74, CD16/32, CD63 or CD14, was confirmed by flow cytometry (**Extended Data Fig.1b**). Gene ontology analyses (**Supplementary Table 2**) indicated involvement of the differentially expressed proteins in immune defense, cytokine signaling and angiogenesis (**Extended Data Fig.1c**). Night-like neutrophils were enriched for pathways linked to c-Kit signaling and platelet production, possibly reminiscent of their time in the bone marrow, as well as GTPase Rho signaling (**Fig. 1b**), consistent with the enhanced migratory capacity of “younger” neutrophils [12]. Day-like neutrophils showed upregulation of protein synthesis, pathogen sensing and respiration (**Fig. 1b**), suggesting specialization for effector functions and enhanced TLRs signaling, as suggested [12, 19]. Comparison of the neutrophil proteome with transcriptional datasets associated with diurnal time[12] showed poor correlation (**Extended Data Fig. 1d**), suggesting that the proteomic changes are not driven by direct transcriptional regulation. These results therefore identify prominent changes in the neutrophil proteome that are associated with the time spent in the circulation.

Circulating neutrophils degranulate in the steady-state

The proteomic data indicated that proteins stored in the various types of granules (azurophilic, specific and tertiary/gelatinase granules) were enriched in night-like neutrophils (**Fig. 1c and**

Supplementary Table 3). An enrichment in granule proteins was also detected in the proteome of circulating neutrophils from AMD3100-mobilized mice compared to day-time neutrophils (**Extended Data Fig. 1e,f** and **Supplementary Table 4**). Further analysis in the Reactome database indicated that proteins differentially detected in the night- vs. day-like groups were associated with degranulation (**Extended Data Fig. 2a**), altogether suggesting progressive loss of granules as neutrophils circulate.

Cytometric analysis of WT circulating neutrophils purified every 4 hours (daytime ZT1, 5 and 9; nighttime ZT13, 17 and 21) revealed circadian oscillations of side-scatter properties, a feature that reflects cell granularity (**Extended Data Fig. 2b**). To assess if these variations in side-scatter were caused by degranulation, we stained cytospins of $Ly6G^+$ blood neutrophils purified at the same times as above for MPO, a protein of azurophilic granules, and analyzed granule content by high-resolution confocal microscopy (**Fig. 1d**). The maximal abundance of MPO^+ granules was observed at ZT17 (midnight, when neutrophils leave the marrow), while the valley was at ZT1 (**Fig. 1e** and **Extended Data Fig. 2c**), indicating progressive loss of primary granules. MPO+ granule content in neutrophils was in anti-phase with elastase activity in plasma (**Fig. 1f**), suggesting release of granule content into blood. A 12-hour shift in the animal light cycle for three weeks completely re-adjusted the pattern of granule content in neutrophils (**Extended Data Fig. 2d)**, indicating that degranulation was circadian in nature. Finally, $Ly6G^+$ neutrophils from lungs, spleen and liver had a lower MPO+ granule content compared to $Ly6G^+$ neutrophils in the blood (**Extended Data Fig. 2e-f**), altogether suggesting that neutrophils undergo homeostatic degranulation in the circulation before they enter tissues.

Neutrophils progressively lose NET-forming capacity

Proteases stored in the azurophilic granules degrade the nuclear histones and promote chromatin decondensation during NET formation [20] and granule proteins have been identified in the NET proteome [21]. Among the proteins found in the proteomic analyses, those associated with NETs (**Supplementary table 3**) were enriched in the proteome of night-like neutrophils (**Fig. 2a**), suggesting that NET release is more prevalent at this time. To directly examine whether the formation of NETs varied during the course of a day, we treated $Ly6G^+$ neutrophils purified at ZT5 or ZT13 from the blood of WT mice with phorbol myristate acetate (PMA), a NET-inducing compound, and analyzed for the presence of extracellular DNA decorated with MPO protein and citrullinated histone 3 (cit-H3). We found that neutrophils at night (ZT13)

formed more NETs than at daytime (ZT5) (**Fig. 2b**), revealing a correlation between diurnal azurophilic granule content and NET-forming capacity in blood Ly6G^{+} neutrophils. Next, we assessed the presence of NETs by whole mount immunostaining with the same markers in cremaster muscles of wild-type and Lyz2^{Cre}Mcl1$^{fl/fl}$ mice (which are neutropenic[22]) after ischemia-reperfusion. Many more NETs were detectable in the muscles of mice at ZT13 than at ZT5, while no NETs were detected in the Lyz2^{Cre}Mcl1$^{fl/fl}$ mice (**Fig. 2c**). Thus, proteomic changes and degranulation of circulating neutrophils temporally coincide with loss of NET-forming ability.

Proteome changes are driven by CXCR2 and Bmal1

Diurnal changes in neutrophil transcription and migration are controlled by a cell-intrinsic mechanism, in which the expression of the chemokine *Cxcl2* is regulated by the molecular clock protein Bmal1 and leads to the cell-autonomous, diurnal activation of neutrophils by signaling though CXCR2[12]. We therefore tested whether this mechanism caused the proteome changes. Treatment with CXCL2 induced degranulation in isolated wild-type Ly6G^{+} circulating neutrophils (**Fig. 3a**). Analysis of the granule content of blood neutrophils at ZT5 and ZT13 from *MRP8*^{CRE} *Cxcr2*$^{fl/fl}$ (referred to as CXCR2$^{\Delta N}$ hereafter)[12], which have a neutrophil-specific deficiency in CXCR2, showed no differences in MPO+ granule content or in side scatter properties in blood neutrophils, compared with neutrophils from wild-type mice (**Fig. 3b** and **Extended Data Fig. 2b**). CXCR2$^{\Delta N}$ neutrophils degranulated in response to PMA and LPS (**Extended Data Fig. 3a-b**), indicating that degranulation could be otherwise induced in these cells. We also found a loss of diurnal oscillations in granule content in blood neutrophils from *Cxcl2*$^{-/-}$mice (**Fig. 3b**). Neutrophils from CXCR2$^{\Delta N}$ and *Cxcl2*$^{-/-}$mice also showed no differences in NET formation between ZT5 and ZT13 (**Fig. 3c**). In chimeric mice transplanted with equal mixes of bone marrow from DsRed+ wild-type and *Cxcl2*$^{-/-}$ mice, *Cxcl2*$^{-/-}$ neutrophils had a higher granule content than wild-type neutrophils analyzed at the same time (ZT5; **Fig. 3d**), suggesting that CXCL2 signaled in neutrophils in an autocrine fashion to control granule content.

Circadian expression of *Cxcl2* in neutrophils is controlled by the transcription factor Bmal1[12]. *MRP8*^{CRE} *Arntl*$^{fl/fl}$ mice, which have a neutrophil-specific deletion of *Arntl* (which encodes Bmal1, referred hereafter as Bmal1$^{\Delta N}$) showed no circadian differences in MPO^{+} granule content between ZT5 and ZT13 (**Extended Data Fig. 4a**) and NET formation (**Extended Data Fig. 4b**) in purified Ly6G+ neutrophils from blood compared to neutrophils from wild-type controls,

suggesting that Bmal1 controlled the changes in the neutrophil proteome. Proteome analysis in Ly6G$^+$ neutrophils purified at ZT5 (day) or ZT13 (night) from the blood of Bmal1$^{\Delta N}$ mice (**Extended Data Fig. 4c** and **Supplementary Table 5**) indicated that Bmal1$^{\Delta N}$ neutrophils did not show circadian changes in granule proteins or in NET-associated proteins (**Extended Data Fig. 4d-e**). These data indicated that Bmal1 and signaling through CXCL2-CXCR2 controlled the changes in granule content and the loss in the capacity to form NETs in neutrophils.

The severity of lung injury varies during the day

To test whether the diurnal changes in the neutrophil proteome influenced the outcome of inflammatory responses in tissues, we used a model of endotoxin and antibody-induced acute lung inflammation (ALI)[15, 23], which is dependent on neutrophils and NETs [24, 25, 26] and recapitulates the pulmonary injury observed in transfused patients [27]. We used ALI-prone Balb/c mice, which displayed normal diurnal variations in neutrophil number and phenotype (**Extended Data Fig. 5a-c**) [12].

Lungs from Balb/c mice treated to induce ALI (by intraperitoneal injection of 0.1mg/kg LPS 24 hours before intravenous injection of 0.5 mg/kg of an anti-H2d antibody) showed evidence of NETs defined by staining for MPO, DNA and cit-H3 (**Fig. 4a, Movie 1** and **Movie 2**)[24, 26]. To assess the kinetics of NET formation *in vivo* during ALI, we performed high-speed multichannel intravital imaging of the lung microcirculation [28]. Neutrophils were identified by Ly6G staining, while NET-like structures where identified by the rapid extrusion of Sytox-green-labelled DNA from Ly6G$^+$ neutrophils, as a result of intravenous injection of the dye 5 minutes before imaging (**Fig. 4b** and **Movie 3**). The Sytox-green$^+$ extrusions were inhibited by the PAD4 inhibitor Cl-amidine injected intravenously one hour before ALI induction (**Fig. 4c**), indicating that they represented NETs. Continuous tracking of neutrophil behavior for 40 minutes showed higher release of Sytox-green$^+$ extrusions at ZT13 compared with ZT5 (**Fig. 4c** and **Movie 3**). The enhanced NET production at night was detectable minutes upon induction of ALI and was sustained for the rest of the experiment (**Fig. 4c**). In contrast, the number of Ly6G$^+$ neutrophils was similar at ZT5 and ZT13 in untreated and in Cl-amidine-treated mice (**Extended Data Fig. 6a-c**). Because platelets have been involved in neutrophil activation and NET formation during ALI [15, 25], we assessed their possible involvement in the observed differences between ZT5 and ZT13. We found a sharp increase in the number of platelets in the pulmonary vessels in mice with ALI, however their numbers were comparable at ZT5 and ZT13 (**Extended Data Fig. 6b**),

suggesting that the number of neutrophils or platelets did not influence the diurnal changes in pulmonary NET-formation.

To evaluate the effects of the diurnal changes in NET formation in the inflamed lungs, we measured the kinetics of edema formation, which is caused by infiltration of plasma in the alveolar space. Intravenous injection with Evan's blue after ALI induction at ZT5 indicated a marked increase in pulmonary vascular permeability during ALI, compared to LPS-only treated controls (**Extended Data Fig. 7a**), which was specific to the lungs. We then used computerized tomography (CT) to track the *in vivo* dynamics of edema in mice in which we induced at ZT5 (day) or at ZT13 (night). We found a rapid and sharp increase in water content of the lungs, which occurred earlier and was higher in ZT13- compared with ZT5-induced mice (**Fig. 4d, e**). This correlated with reduced survival of mice in which ALI was induced at ZT13 compared to those induced at ZT5 (**Fig. 4f**). Finally, treatment with Cl-amidine one hour before induction at ZT5 protected mice from edema and death (**Fig. 4e, f**), indicating that the release of NETs was a primary cause of ALI. Thus, the severity of lung injury during ALI displays diurnal patterns that correlate with granule content and capacity to form NETs by neutrophils.

Variations in the neutrophil proteome drive lung injury

To assess whether neutrophil-intrinsic variations in granule content and NET formation caused lung inflammation, we used Bmal1$^{\Delta N}$ mice and *MRP8*^{CRE} *Cxcr4*$^{fl/fl}$, which lacked CXCR4, a negative regulator of CXCR2 signaling[12], specifically in neutrophils (hereafter CXCR4$^{\Delta N}$). Neutrophils from Bmal1$^{\Delta N}$ and CXCR4$^{\Delta N}$ mice share transcriptional and migratory properties with night and day neutrophils, respectively[12]. MPO immunofluorescence and transmission electron microscopy imaging of Ly6G^{+} blood neutrophils purified at ZT5 revealed higher azurophilic granule content in Bmal1$^{\Delta N}$ neutrophils compared with wild-type neutrophils, and comparable to that of wild-type neutrophils at ZT13 (**Fig. 5a,b**). In contrast, CXCR4$^{\Delta N}$ neutrophils at ZT5 had strong reductions in azurophilic granule content compared with WT neutrophils at any time point (**Fig. 5a, b**). NET formation in response to PMA was elevated in Bmal1$^{\Delta N}$ neutrophils obtained at ZT5, and strongly reduced in CXCR4$^{\Delta N}$ neutrophils, relative to wild-type cells at ZT5 (**Fig. 5c**). Thus, variations in granule content and NET formation are driven by a neutrophil-intrinsic program.

To test whether the diurnal changes in the susceptibility to ALI were caused by changes in neutrophil granularity, we analyzed the responses of Bmal1$^{\Delta N}$ and CXCR4$^{\Delta N}$ mice to induction of ALI at ZT5. Intravital microscopy analyses showed faster and elevated NET formation in the lungs of Bmal1$^{\Delta N}$ mice, compared with lungs of CXCR4$^{\Delta N}$ mice, which were similar to the differences found at ZT13 and ZT5, respectively, in wild-type mice (**Fig. 5d**). Intravital microscopy and flow cytometry showed similar numbers of neutrophils and platelets, as well as the number of interactions with each other, within the microvasculature of wild-type, Bmal1$^{\Delta N}$ and CXCR4$^{\Delta N}$ mice (**Extended Data Fig. 6d-g**), indicating an otherwise normal behavior of intravascular neutrophils in these mice. We found dramatically elevations in pulmonary edema and reduced survival in Bmal1$^{\Delta N}$ mice during ALI induced at ZT5, compared with CXCR4$^{\Delta N}$ mice (**Fig. 5e,f** and **Movie S4**). The protection from pathology correlated with preservation of vascular permeability in the lungs of CXCR4$^{\Delta N}$ mice after intravenous injection of Evans blue (**Extended Data Fig. 7b,c**). Intravital imaging in wild-type mice allowed visualization of two distinct NET-like formation events, “flowing” NETs, in which the extruded NETs were immediately washed away by the bloodstream, and “adherent” NETs, in which the extruded DNA remained adherent to the vasculature (**Extended Data Fig. 7d** and **Movie S5**). In Bmal1$^{\Delta N}$ mice, the frequency of adherent NETs was elevated compared with flowing NETs, but not in wild-type or CXCR4$^{\Delta N}$ mice (**Extended Data Fig. 7e**), suggesting that the ability of neutrophils to deposit NETs onto the endothelium enhanced vascular damage in Bmal1$^{\Delta N}$ mice.

Next, we tested the causal relationship between the diurnal proteome changes in neutrophils and the diurnal susceptibility to inflammation in the Bmal1$^{\Delta N}$ mice. Neutrophils from Bmal1$^{\Delta N}$ mice had a constitutively high MPO+ granule content and NET-forming capacity (**Extended Data Fig. 4a,b**), and reduced survival during ALI at both ZT5 or ZT13 (**Extended Data Fig. 8a**). CXCR4$^{\Delta N}$ neutrophils, in turn, had a similar loss in circadian granule content and NET formation (**Extended Data Fig. 8b,c**), and higher survival during ALI at both ZT5 or ZT13 (**Extended Data Fig. 8a**). Of note, the number of circulating neutrophils in Bmal1$^{\Delta N}$ mice oscillated during the day, similar to wild-type mice (**Extended Data Fig. 8d**), whereas CXCR4$^{\Delta N}$ mice display constitutively high neutrophil counts[12], indicating that the granule content, but not the number of neutrophils, was associated with the severity of pulmonary inflammation. These observations indicated that impaired diurnal changes in the proteome and the granule content in neutrophils were related to the magnitude of inflammation.

Human neutrophils undergo proteome disarming

Clinical manifestations of inflammation display circadian oscillations in humans, and are associated with time-of-day variations in both the incidence and the severity of cardiovascular disease [29, 30, 31]. We tested whether neutrophil "disarming" in humans could underlie the circadian changes in vascular inflammation. In 10 healthy volunteers we measured neutrophil counts in blood and performed proteomic analysis, granule content and NET formation assays in neutrophils isolated at 8 am, 2 pm and 7 pm (**Extended Data Fig. 9a**), when diurnal patterns in neutrophil number and phenotype are prominent in humans[12]. Human neutrophils display a night-like phenotype (similar to murine ZT13) early in the morning and progress towards a day-like phenotype (similar to murine ZT5) over the next 4-8 hours [12]. In our cohort, neutrophil counts increased over time and peaked at 2-7 pm (**Fig. 6a**), while the granularity of neutrophils, indicated by the side scatter by flow cytometry, decreased from 8 am to 7 pm (**Fig. 6b**). Direct examination of granules in human neutrophils stained for MPO (**Fig. 6c-d**), as well as by TEM imaging (**Fig. 6e**), indicated a diurnal reduction in granule content, which peaked at 8 am and showed a trough at 2 pm.

Proteomic analyses of neutrophils isolated in density gradients at 8 am and 2 pm from the blood of 5 healthy volunteers (**Supplementary Table 6**) indicated that, from a total of 1918 proteins detected, around 9.7% were differentially enriched when comparing 8am versus 2pm ($p < 0.05$; **Fig. 6f**). Gene ontology analyses revealed that the differentially detected proteins were in pathways related to vesicle-mediated transport, secretion, exocytosis or degranulation (**Extended Data Fig. 9b** and **Supplementary Table 7**), consistent with a loss of granule content in human neutrophils over time. Many of the individual proteins identified in the mouse analyses were not detected, or did not show diurnal changes, in the human samples (not shown), probably indicating a high variability among human individuals compared with co-housed and strain-matched mice. However, numerous granule proteins, such as MPO, MMP9, or LTF, were more abundant at 8am than at 2 pm in human neutrophils (**Fig. 6g**). Similar to mouse neutrophils, there was a poor correlation between transcript and protein amounts in human neutrophils (**Extended Data Fig. 9c**), suggesting that the proteomic changes were largely independent of transcriptional regulation. *Ex vivo* assays of human neutrophils purified using density gradients and treated with vehicle or PMA indicated a marked reduction in NET-forming capacity between 8 am and 2 pm (**Fig. 6h-i**), corresponding with more NET-related proteins at 8am compared to 2 pm (**Extended Data Fig. 9d**). These observations suggested that diurnal degranulation also occurred in circulating human neutrophils.

We finally tested whether the changes in proteome, granule content and NET-forming activity in human neutrophils were associated with variations in the susceptibility to develop inflammation, and/or its severity. We focused on an existing cohort of 5334 patients with community-acquired pneumonia (CAP), which are at risk of developing acute respiratory distress syndrome (ARDS) [32]. Retrospective analysis of the human cohort indicated that, among the patients hospitalized with CAP, 125 (2.3%) developed ARDS. Assessment of the temporal patterns of disease onset and severity (using the pneumonia severity index) by plotting the times of admission against the pneumonia index and death in this subset of patients revealed consistent diurnal oscillations, with a peak around 9 am and a trough at 5-7 pm for both parameters (**Fig. 6j**). These observations indicate that proteomic disarming occurs in human neutrophils and may influence the incidence and severity of inflammation (**Extended Data Fig.10** and **MovieS6**).

Discussion

Here, we describe the existence in neutrophils of a cell-intrinsic program that induced the progressive loss of granule proteins involved in inflammation and the formation of NETs and provided a previously unrecognized layer of protection against the toxic activity of these leukocytes. The phenomenon of proteome disarming described herein shared key features with the process of neutrophil "aging" [12], in terms of reliance on CXCR2 signaling, regulation by Bmal1 and CXCR4 in a cell-intrinsic manner and similar temporal patterns (i.e., peak at noon). This suggested that neutrophil aging and disarming might represent distinct manifestations of a core circadian program in neutrophils that allows anticipation of potential threats[12], but also protects from excessive inflammation, vascular damage and death.

Beyond regulating the magnitude of inflammation, changes in the neutrophil proteome displayed temporal oscillations that aligned neutrophil activity with circadian cycles. The circadian transcriptional regulation of migration-associated genes by Bmal1 controls the migratory properties of neutrophils, and allows the infiltration of naïve tissues in anticipation of potential infections [12]. In addition to these transcription-mediated mechanisms, we uncovered here that the neutrophil proteome is also subject to circadian regulation, which blunts the ability of neutrophils to release toxic mediators and to produce NETs. This level of immune regulation may be particularly relevant for granulocytes, a group of innate immune cells that synthesize and store the majority of their early-response mediators inside dedicated organelles. Because the formation of granules and their content occurs as neutrophils differentiate in the bone

marrow [7, 33], it is unlikely that changes of the granule proteome that occur in the circulation are transcriptionally regulated, as illustrated by the poor correlation between the proteome and the transcriptome in these cells. Our data, however, suggested a model in which upstream control of transcription of *Cxcl2* by Bmal1 [12] allowed indirect regulation of the neutrophil proteome by the canonical circadian machinery. Conceptually, the temporal nature of this process in blood aligns with the evolutionary value of circadian oscillations in segregating mutually antagonistic processes, in this case potent anti-microbial responses and protection of the host against immune-mediated damage.

The circadian patterns in the granule content and elastase activity in plasma suggested the progressive discharge of granules while in the circulation, such that neutrophils that migrate into tissues during the day [10] would have lost part of their anti-microbial arsenal, and would be as such less likely to elicit organ damage, as shown in the mouse model of ALI. Because neutrophil proteases are also important for the activation of many biological mediators, including cytokines, chemokines, growth factors and adhesion and pattern-recognition receptors [34, 35], and even modulate signaling cascades in other cells [36, 37], the programmed proteome changes reported here may have pleiotropic consequences in physiology. For instance, it predicts that neutrophils that are newly released from the bone marrow in conditions of stress, such as obesity or cancer [38, 39], may be better suited to regulate physiological aspects of target organs than the aged neutrophils that enter the tissues at the end of their life cycle and have lost part of their cargo.

Our observations shed light into the particular susceptibility of the lungs to diurnal inflammation. Large numbers of neutrophils accumulate within the pulmonary microcirculation in mice, rabbits and non-human primates after stimulation or in the steady-state [10, 18, 40], and the lungs can provide a niche for effective anti-microbial responses [41]. The homeostatic accumulation of neutrophils in the lungs at the end of the light cycle in mice [10] would predict higher susceptibility to inflammatory stimuli at this time. However, we found that neutrophils recovered from naïve lungs had reduced granularity, and that mutant mice with constitutive low levels of granules in neutrophils displayed permanent protection from ALI, suggesting a dominant contribution of the disarming process in tissue protection.

It has long been recognized that multiple inflammatory processes in humans display circadian periodicity [42], and experimental models and retrospective studies have corroborated that not only the onset of inflammation, but also the severity of the inflammatory events manifest diurnal oscillations [31]. These events are often caused by neutrophil activation and by thrombosis, which

in turn can be exacerbated in the presence of neutrophils or NETs [15, 25, 43, 44]. Thus, our current findings in the context of ALI may extend to other inflammatory and thrombotic conditions affecting multiple organs, and suggest that interventions aimed at inducing controlled degranulation may effectively "disarm" neutrophils and protect organs from catastrophic inflammation.

Supplementary Information

The Supplementary Information file contains Extended Data Figures 1-10 and legends for Movies S1-6 and Supplementary Tables 1-8.

Acknowledgments

We thank members of the Comparative Medicine Unit and Advanced microscopy Unit at CNIC. This study was supported by Intramural grants from the Severo Ochoa program (IGP-SO), grant from Fundació La Marató de TV3 (120/C/2015-20153032), grant SAF2015-65607-R from Ministerio de Ciencia, Investigacion y Universidades (MCIU) with co-funding by Fondo Europeo de Desarrollo Regional (FEDER), RTI2018-095497-B-I00 from MCIU, and HR17_00527 from Fundación La Caixa to A.H. Fellowship BES-2013-065550 from MCIU to J.M.A, fellowship from La Caixa Foundation (ID 100010434) code LCF/BQ/DR19/11740022 for A.A-C., and fellowship Health-PERIS 2016–2020 to C.C. Funds were also obtained from Instituto de Salud Carlos III (ISCIII) FIS PI17/01601 to I.L. and SAF2015-68632-R from MCIU to M.A.M.; Welcome Trust Seed Award in Science (206103/Z/17/Z) to D.R., SFB1123-A1/A10 from Deutsche Forschungsgemeinschaft and ERC-AdG 692511 to C.W. ; SAF2017-84494-C2-R and Programa Red Guipuzcoana de Ciencia, Tecnología e Información 2018-CIEN-000058-01 to J.R-C. Work at CIC biomaGUNE was performed under the Maria de Maeztu Units of Excellence Program from the Spanish State Research Agency (MDM-2017-0720). The CNIC is supported by the MCIU and the Pro-CNIC Foundation, and is a Severo Ochoa Center of Excellence (MEIC award SEV-2015-0505).

Author contribution: J.M.A, A.A.C, G.C., E.B.K., E.C., and Y.R.V. performed experiments. J.M.A., D.R. and A.R.P. performed bioinformatic analysis. F.O. obtained human samples. C.W., M.A.M., J.R-C., I.L. and J.V. contributed essential reagents, equipment, expertise and funds. C.C. and A.T. contributed clinical data. J.M.A. and A.H. designed and supervised experiments, and wrote the manuscript, which was edited by all authors.

Author Information: Reprints and permissions information are available at www.nature.com/reprints. The authors declare no competing financial interests. Correspondence and requests for materials should be addressed to ahidalgo@cnic.es

References

1. Cowland JB, Borregaard N. Granulopoiesis and granules of human neutrophils. *Immunol Rev* 2016, **273**(1)**:** 11-28.

2. Ley K, Hoffman HM, Kubes P, Cassatella MA, Zychlinsky A, Hedrick CC*, et al.* Neutrophils: New insights and open questions. *Sci Immunol* 2018, **3**(30).

3. Borregaard N, Sorensen OE, Theilgaard-Monch K. Neutrophil granules: a library of innate immunity proteins. *Trends Immunol* 2007, **28**(8)**:** 340-345.

4. Rorvig S, Ostergaard O, Heegaard NH, Borregaard N. Proteome profiling of human neutrophil granule subsets, secretory vesicles, and cell membrane: correlation with transcriptome profiling of neutrophil precursors. *J Leukoc Biol* 2013, **94**(4)**:** 711-721.

5. Borregaard N. Neutrophils, from marrow to microbes. *Immunity* 2010, **33**(5)**:** 657-670.

6. Le Cabec V, Cowland JB, Calafat J, Borregaard N. Targeting of proteins to granule subsets is determined by timing and not by sorting: The specific granule protein NGAL is localized to azurophil granules when expressed in HL-60 cells. *Proc Natl Acad Sci U S A* 1996, **93**(13)**:** 6454-6457.

7. Evrard M, Kwok IWH, Chong SZ, Teng KWW, Becht E, Chen J*, et al.* Developmental Analysis of Bone Marrow Neutrophils Reveals Populations Specialized in Expansion, Trafficking, and Effector Functions. *Immunity* 2018, **48**(2)**:** 364-379 e368.

8. Grassi L, Pourfarzad F, Ullrich S, Merkel A, Were F, Carrillo-de-Santa-Pau E*, et al.* Dynamics of Transcription Regulation in Human Bone Marrow Myeloid Differentiation to Mature Blood Neutrophils. *Cell Rep* 2018, **24**(10)**:** 2784-2794.

9. Tak T, Tesselaar K, Pillay J, Borghans JA, Koenderman L. What's your age again? Determination of human neutrophil half-lives revisited. *J Leukoc Biol* 2013, **94**(4)**:** 595-601.

10. Casanova-Acebes M, Nicolas-Avila JA, Li JL, Garcia-Silva S, Balachander A, Rubio-Ponce A*, et al.* Neutrophils instruct homeostatic and pathological states in naive tissues. *J Exp Med* 2018, **215**(11)**:** 2778-2795.

11. He W, Holtkamp S, Hergenhan SM, Kraus K, de Juan A, Weber J*, et al.* Circadian Expression of Migratory Factors Establishes Lineage-Specific Signatures that Guide the Homing of Leukocyte Subsets to Tissues. *Immunity* 2018, **49**(6)**:** 1175-1190 e1177.

12. Adrover JM, Del Fresno C, Crainiciuc G, Cuartero MI, Casanova-Acebes M, Weiss LA*, et al.* A Neutrophil Timer Coordinates Immune Defense and Vascular Protection. *Immunity* 2019.

13. Grommes J, Soehnlein O. Contribution of neutrophils to acute lung injury. *Mol Med* 2011, **17**(3-4)**:** 293-307.

14. Looney MR, Su X, Van Ziffle JA, Lowell CA, Matthay MA. Neutrophils and their Fc gamma receptors are essential in a mouse model of transfusion-related acute lung injury. *The Journal of clinical investigation* 2006, **116**(6)**:** 1615-1623.

15. Sreeramkumar V, Adrover JM, Ballesteros I, Cuartero MI, Rossaint J, Bilbao I*, et al.* Neutrophils scan for activated platelets to initiate inflammation. *Science* 2014, **346**(6214)**:** 1234-1238.

16. Matthay MA, Zemans RL. The acute respiratory distress syndrome: pathogenesis and treatment. *Annual review of pathology* 2011, **6:** 147-163.

17. Casanova-Acebes M, Pitaval C, Weiss LA, Nombela-Arrieta C, Chevre R, N AG*, et al.* Rhythmic modulation of the hematopoietic niche through neutrophil clearance. *Cell* 2013, **153**(5)**:** 1025-1035.

18. Devi S, Wang Y, Chew WK, Lima R, N AG, Mattar CN*, et al.* Neutrophil mobilization via plerixafor-mediated CXCR4 inhibition arises from lung demargination and blockade of neutrophil homing to the bone marrow. *J Exp Med* 2013, **210**(11)**:** 2321-2336.

19. Zhang D, Chen G, Manwani D, Mortha A, Xu C, Faith JJ*, et al.* Neutrophil ageing is regulated by the microbiome. *Nature* 2015, **525**(7570)**:** 528-532.

20. Papayannopoulos V, Metzler KD, Hakkim A, Zychlinsky A. Neutrophil elastase and myeloperoxidase regulate the formation of neutrophil extracellular traps. *J Cell Biol* 2010, **191**(3)**:** 677-691.

21. Urban CF, Ermert D, Schmid M, Abu-Abed U, Goosmann C, Nacken W*, et al.* Neutrophil extracellular traps contain calprotectin, a cytosolic protein complex involved in host defense against Candida albicans. *PLoS Pathog* 2009, **5**(10)**:** e1000639.

22. Csepregi JZ, Orosz A, Zajta E, Kasa O, Nemeth T, Simon E*, et al.* Myeloid-Specific Deletion of Mcl-1 Yields Severely Neutropenic Mice That Survive and Breed in Homozygous Form. *Journal of immunology* 2018, **201**(12)**:** 3793-3803.

23. Looney MR, Nguyen JX, Hu Y, Van Ziffle JA, Lowell CA, Matthay MA. Platelet depletion and aspirin treatment protect mice in a two-event model of transfusion-related acute lung injury. *The Journal of clinical investigation* 2009, **119**(11)**:** 3450-3461.

24. Caudrillier A, Kessenbrock K, Gilliss BM, Nguyen JX, Marques MB, Monestier M*, et al.* Platelets induce neutrophil extracellular traps in transfusion-related acute lung injury. *The Journal of clinical investigation* 2012, **122**(7)**:** 2661-2671.

25. Hidalgo A, Chang J, Jang JE, Peired AJ, Chiang EY, Frenette PS. Heterotypic interactions enabled by polarized neutrophil microdomains mediate thromboinflammatory injury. *Nat Med* 2009, **15**(4)**:** 384-391.

26. Thomas GM, Carbo C, Curtis BR, Martinod K, Mazo IB, Schatzberg D*, et al.* Extracellular DNA traps are associated with the pathogenesis of TRALI in humans and mice. *Blood* 2012, **119**(26)**:** 6335-6343.

27. Looney MR, Gilliss BM, Matthay MA. Pathophysiology of transfusion-related acute lung injury. *Current opinion in hematology* 2010, **17**(5)**:** 418-423.

28. Looney MR, Thornton EE, Sen D, Lamm WJ, Glenny RW, Krummel MF. Stabilized imaging of immune surveillance in the mouse lung. *Nature methods* 2011, **8**(1)**:** 91-96.

29. Muller JE, Stone PH, Turi ZG, Rutherford JD, Czeisler CA, Parker C*, et al.* Circadian variation in the frequency of onset of acute myocardial infarction. *The New England journal of medicine* 1985, **313**(21)**:** 1315-1322.

30. Scheiermann C, Kunisaki Y, Frenette PS. Circadian control of the immune system. *Nat Rev Immunol* 2013, **13**(3)**:** 190-198.

31. Suarez-Barrientos A, Lopez-Romero P, Vivas D, Castro-Ferreira F, Nunez-Gil I, Franco E*, et al.* Circadian variations of infarct size in acute myocardial infarction. *Heart* 2011, **97**(12)**:** 970-976.

32. Cilloniz C, Ferrer M, Liapikou A, Garcia-Vidal C, Gabarrus A, Ceccato A*, et al.* Acute respiratory distress syndrome in mechanically ventilated patients with community-acquired pneumonia. *Eur Respir J* 2018, **51**(3).

33. Faurschou M, Borregaard N. Neutrophil granules and secretory vesicles in inflammation. *Microbes Infect* 2003, **5**(14)**:** 1317-1327.

34. Meyer-Hoffert U. Neutrophil-derived serine proteases modulate innate immune responses. *Front Biosci (Landmark Ed)* 2009, **14:** 3409-3418.

35. Pham CT. Neutrophil serine proteases: specific regulators of inflammation. *Nat Rev Immunol* 2006, **6**(7)**:** 541-550.

36. Houghton AM, Rzymkiewicz DM, Ji H, Gregory AD, Egea EE, Metz HE*, et al.* Neutrophil elastase-mediated degradation of IRS-1 accelerates lung tumor growth. *Nat Med* 2010, **16**(2)**:** 219-223.

37. Talukdar S, Oh DY, Bandyopadhyay G, Li D, Xu J, McNelis J*, et al.* Neutrophils mediate insulin resistance in mice fed a high-fat diet through secreted elastase. *Nat Med* 2012, **18**(9)**:** 1407-1412.

38. Coffelt SB, Kersten K, Doornebal CW, Weiden J, Vrijland K, Hau CS*, et al.* IL-17-producing gammadelta T cells and neutrophils conspire to promote breast cancer metastasis. *Nature* 2015, **522**(7556)**:** 345-348.

39. Quail DF, Olson OC, Bhardwaj P, Walsh LA, Akkari L, Quick ML*, et al.* Obesity alters the lung myeloid cell landscape to enhance breast cancer metastasis through IL5 and GM-CSF. *Nat Cell Biol* 2017, **19**(8)**:** 974-987.

40. Doerschuk CM. The role of CD18-mediated adhesion in neutrophil sequestration induced by infusion of activated plasma in rabbits. *American journal of respiratory cell and molecular biology* 1992, **7**(2)**:** 140-148.

41. Yipp BG, Kim JH, Lima R, Zbytnuik LD, Petri B, Swanlund N*, et al.* The Lung is a Host Defense Niche for Immediate Neutrophil-Mediated Vascular Protection. *Sci Immunol* 2017, **2**(10).

42. Muller JE, Tofler GH. Circadian variation and cardiovascular disease. *The New England journal of medicine* 1991, **325**(14)**:** 1038-1039.

43. Engelmann B, Massberg S. Thrombosis as an intravascular effector of innate immunity. *Nat Rev Immunol* 2013, **13**(1)**:** 34-45.

44. Jimenez-Alcazar M, Rangaswamy C, Panda R, Bitterling J, Simsek YJ, Long AT*, et al.* Host DNases prevent vascular occlusion by neutrophil extracellular traps. *Science* 2017, **358**(6367)**:** 1202-1206.

Figure legends

Figure 1. Diurnal changes in the neutrophil proteome.

a, Volcano plot of total the total proteome showing proteins with a False Discovery Rate (FDR) < 0.01 (calculated as stated in methods section, from single samples of 60 million neutrophils pooled from 9 mice (night) and 6 mice (day). A positive Z-score represents an increase in nighttime (fresh) over daytime (aged) neutrophils. Color represents the functional category for each protein (legend, top-right). **b**, Gene-set enrichment analysis of the proteomics data showing pathways with a p-value < 0.15 enriched in aged (red) or fresh (blue) neutrophils. Size of the bubble-plot represents overlap between query and gene-set (legend bottom-right). **c**, Volcano plot of the proteomic dataset showing granule proteins with a Z-score > 2. Colors show the granule type for each protein (top right). **d**, Z-stack maximum projection of neutrophils stained for primary granules with MPO and counterstained with DAPI. **e**, Quantification of neutrophil granule contents during a full diurnal cycle. Curves are repeated (dashed line) to better appreciate the circadian pattern. Dark phase is shown in grey; n=30 cells per time point. **f**, Neutrophil elastase activity in plasma. Curves are repeated (dashed line) to better appreciate the circadian pattern. Dark phase is shown in grey; n=4 mice per time point. Data in e and f, are shown as mean ± SEM, and circadian oscillation p-values were determined by amplitude vs. zero two-tailed two-tailed t-test analysis (see Methods).

Figure 2. Diurnal loss of NET-forming capacity.

a, Volcano plot of the neutrophil proteome showing proteins found in NETs (red dots), and enrichment of these proteins in nighttime neutrophils. **b**, *Ex vivo* NET-formation assay. Neutrophils sorted at ZT13 (nighttime) or ZT5 (daytime) were stimulated with PMA or vehicle to induce NETs and stained for citrunillated-histone 3 (Cit-H3) and DNA (left). Colocalization of both markers was used to quantify NET formation as shown in the bar graph (right); n=3 mice per time point. **c**, Representative images (left) and quantification (right) of in vivo NET formation in the cremaster muscle subjected to ischemia/reperfusion at nighttime (ZT13), or at daytime (ZT5). Triple colocalization of MPO, DNA and Cit-H3 was used to define and quantify the area of NETs (red; arrowheads). Neutropenic $Mcl1^{\Delta N}$ mice ($Lyz2^{Cre}$; $Mcl1^{fl/fl}$ mice) were used as controls and showed no NETs. Dotted areas are showed magnified in bottom panels; n = 3 mice per condition. Scale bars, 50 μm. Bars show mean ± SEM. *; p<0.05; n.s., not significant, as determined by unpaired two-tailed t-test analysis.

Figure 3. Degranulation and loss of NET-forming capacity are driven by CXCL2/CXCR2 signaling.

a, Ex-vivo stimulation of sorted neutrophils with CXCL2 induces degranulation (right), as quantified by confocal imaging of MPO-stained neutrophils (left); n = 29 (--) and 32 (+) cells. **b**, Diurnal quantification of granule content in neutrophils from WT, $CXCR2^{\Delta N}$ or $CXCL2^{-/-}$ mice, showing a loss of diurnal fluctuation in CXCR2-deficient (n = 38 cells at ZT5 and 40 cells at ZT13) or CXCL2-deficient neutrophils (n = 31 cells at ZT5 and 14 cells at ZT13), compared to their WT

counterparts (n = 30 cells at ZT5 and 34 cells at ZT13). **c**, Ex-vivo NET formation assays with sorted neutrophils stimulated with PMA or vehicle control, at nighttime (ZT13) or daytime (ZT5). NETs were quantified by triple-colocalization of citrunillated-histone 3, DNA and MPO in confocal micrographs (left; scale bar, 25 μm). Each mouse was normalized to its vehicle control and NET formation at ZT13 and ZT5 compared (right). CXCL2-deficient (n = 3 mice per time) and CXCR2-deficient (n = 6 mice at ZT5 and 2 mice at ZT13) neutrophils showed loss of diurnal fluctuation in NET formation compared with WT cells (n = 6 mice at ZT5 and 4 mice at ZT13). **d**, CXCL2 signaling causes degranulation cell-autonomously, as shown by analysis of MPO+ granules in neutrophils from BM chimeras reconstituted with DsRed+ wild-type and $DsRed^{NEG}$ *Cxcl2*$^{-/-}$ donors; scale bar, 5 μm; n = 3 mice. Bars show mean ± SEM. **; p<0.01; n.s., not significant, as determined by paired (a,d) or unpaired (b-c) two-tailed t-test analysis.

Figure 4. Diurnal loss of NET formation and pulmonary protection during ALI.
a, Presence of NETs in lungs. Shown are maximum projections of confocal Z-stack series of cleared lungs from control mice (Basal) or mice with antibody-induced acute lung injury induction (ALI). Lungs were stained against citrunillated-histone 3, MPO and DNA, and some NETs are shown (arrowheads). Scale, 30 μm. Representative images of n = 3 cleared lungs per condition. **b**, Time-series of 4D intravital imaging captures of NET-like structures in the lungs of ALI-induced mice. NET-like structures were defined as free DNA extruded out of Ly6G+ neutrophils. See also **Movie 1. c**, Quantification of NET-like structures as shown in b, and normalized to the number of neutrophils in mice in which ALI was performed at nighttime (ZT13, blue line) or daytime (ZT5, red line), or in mice treated with Cl-amidine (at ZT5, dashed gray line). Time course (left panel) and area under the curve values (right panel); in both, n = 15 fields from 4 mice per condition. Individual data points are not shown here as this graph uses a mean ± SEM value for the area under the curve calculated from the data shown in the left panel. **d**, Representative images of longitudinal CT series of edema formation at 0 or 21 min after inducing ALI ZT13 or ZT5. Note the increased edema (red) at night. Background bone signal (grey) is shown for anatomical positioning. **e**, Quantification of the images in d. Volume of edema was increased at ZT13 (blue; n = 7 mice) relative to ZT5 (red; n = 7 mice). Mice treated with Cl-amidine are shown as a control (grey, n = 4 mice). **f**, Survival of mice subjected to ALI at ZT13 (blue, n = 18 mice) or ZT5 (red, n = 21 mice), or treated with Cl-amidine (gray, n = 11 mice). Data are shown as mean ± SEM. **; p<0.01; ***, p<0.001, as determined by one-way ANOVA with Dunnet's multiple comparison test (c), two-way ANOVA (eE) or log rank (two-tailed Mantel-Cox) test (f).

Figure 5. Diurnal degranulation and pulmonary protection is neutrophil-intrinsic.
a, Confocal micrographs and quantification of primary granules in neutrophils from WT mice at night (ZT13, n = 33 cells from 3 mice) or daytime (ZT5, n = 30 cells from 3 mice), and from mutant mice (n = 50 cells from 3 $CXCR4^{\Delta N}$ mice and 41 cells from 3 $Bmal1^{\Delta N}$ mice, both at ZT5); scale, 2 μm; **b**, Transmission electron microscopy images (left), and quantification of electrodense azurophilic granules (right) in WT and mutant mice (all at ZT5), showing increased granule content in $Bmal1^{\Delta N}$, and reduced in $CXCR4^{\Delta N}$ neutrophils compared with WT cells; n = 19 cells from 3 mice each; scale, 1 μm. **c**, *Ex vivo* NET formation in sorted WT, $Bmal1^{\Delta N}$ or $CXCR4^{\Delta N}$ neutrophils stimulated with PMA or vehicle as control; n = 3 mice per condition. **d**, Quantification of NET-like

structures normalized to the number of neutrophils during ALI in Bmal1$^{\Delta N}$ (purple line) or CXCR4$^{\Delta N}$ (blue line) mice. Time course and elevations from baseline (gray area) are shown in the left panel, and the areas under the curve are shown in the right panel (Individual data points are not shown here as this graph uses a mean ± SEM value for the area under the curve calculated from the data shown in the left panel). Experiments were performed at ZT5. Data from wild-type mice at ZT5 (light gray, dashed) and ZT13 (dark gray, dashed) from **Fig. 4c** are shown for reference; n = 15 fields from 3 mice for each condition. **e**, Representative images of longitudinal CT series of edema (red) in mutant mice subject to ALI (left) at ZT5, and quantification of the edema volume over time (right panel); n = 7 mice per genotype. **f**, Survival curves of Bmal1$^{\Delta N}$ (n = 19 mice) and CXCR4$^{\Delta N}$ (n = 12 mice) mice subjected to ALI at ZT5. Data are shown as mean ± SEM. *; p<0.05; **, p<0.01; ***, p<0.001; n.s., not significant, as determined by one-way ANOVA with Dunnet's multiple comparison test (a-d), two-way ANOVA (e) or two-sided log rank (Mantel-Cox) test (f).

Figure 6. Evidence for neutrophil disarming and pulmonary protection in humans.

a, Blood neutrophil counts in human volunteers at the different time points; n = 10 human volunteers per timepoint. **b**, Light scattering (SSC-A) values for human neutrophils at different times, as measured by flow cytometry; n = 10 human volunteers. **c**, Quantification of primary granules from confocal images of human neutrophils from images in d; n = 150 cells from 10 volunteers per time point. **d**, Representative images of granule content of human neutrophils, quantified in c. **e**, Transmission electron micrographs (left) of human neutrophils in the morning (8 am) and early afternoon (2 pm), and quantification (right) showing reduced numbers of electrodense primary granules; n = 33 cells from 3 human volunteers per time point. **f**, Volcano plot of the human neutrophil proteome analyzed at 8am and 2pm, showing proteins with p-value < 0.001 (see Methods section for human TMT proteomics). A negative Z-score represents higher values at 8am over 2pm neutrophils. n = 5 per time point. **g**, Volcano plot of granule proteins in the human neutrophil proteome, showing higher content in granule proteins (color-coded) at 8 am compared with 2 pm; n = 5 samples from healthy volunteers. Red dots and labels show differentially expressed proteins with p-value<0.05, and black dots show all granule proteins. Label color indicates the granule type in which the protein is normally found (top right). **h**, Representative confocal images and **i**, quantification of *ex vivo* NET formation by human neutrophils stimulated with PMA or vehicle at the indicated time points. n = 10 volunteers per time point. **j**, Acute respiratory distress syndrome (ARDS) severity shown as the pneumonia severity index (left) and intra-hospitalary deaths (right), of patients entering the ICU at different times of the day; n = 125 patients. Data are shown as mean ± SEM. **; p<0.01, as determined by unpaired two-tailed t-test analysis (f). P values for the circadian plots were calculated by the amplitude vs. zero two-tailed t-test analysis (a-c, g, i). Maroon line in a-c, g and i shows the non-linear COSINOR fit of the data.

Methods

Mice

All experiments were performed in 7-18 weeks old male C57BL/6 or Balb/c mice kept in a specific pathogen-free facility at Centro Nacional de Investigaciones Cardiovasculares (CNIC) under a 12h light/12h dark schedule (lights on at 7am, off at 7pm), with water and chow available ad libitum. Bmal1$^{\Delta N}$, CXCR4$^{\Delta N}$ and CXCR2$^{\Delta N}$ mutants in the C57BL/6 background have been described [12]. For the ALI experiments, Bmal1$^{\Delta N}$ and CXCR4$^{\Delta N}$ mice were backcrossed into the Balb/c background for at least 6 generations and we confirmed susceptibility to antibody-induced lung injury at this stage (not shown). All procedures with backcrossed mice were controlled using Cre-negative littermates. For bone marrow transplant experiments, WT donor bone marrow came from mice expressing DsRed under the control of the β-actin promoter (DsRed^{Tg}). No specific randomization method was followed in this study. All experimental procedures were approved by the Animal Care and Ethics Committee of CNIC and the regional authorities.

Proteomic analysis of fresh and aged mouse neutrophils with ^{18}O

Neutrophils were obtained from the blood of C57BL6 mice using different strategies. For night-like neutrophils, mice were treated with AMD3100 (2.5 mg/kg i.p.) 1h before collection. For day-like neutrophils, mice were treated with anti-P/E-selectin antibodies (1mg/kg i.v.) for 5d, every other day, before collection. Blood was obtained by collection in EDTA tubes to prevent coagulation. RBCs were precipitated using methylcellulose and leukocytes in the top phase were collected and washed before purification by negative selection. Negative selection was performed by incubation with biotinylated antibodies against CD3e, TER119, B220, CD8, CD115, CD4, CD49b and CD117, then incubated with streptavidin-coated beads and applied in a magnet for negative selection of neutrophils. We obtained neutrophils with a purity over 84%. 60 million neutrophils from each source were obtained for analysis.

After in-gel trypsin digestion, the “night-like” samples were equally mixed with the “day-like” samples which were labelled with 18O. The resulting tryptic peptide mixtures were subjected to nano-liquid chromatography coupled to mass spectrometry for protein identification. Peptides were injected onto a C-18 reversed phase (RP) nano-column (75 µm I.D. and 50 cm, Acclaim PepMap100, Thermo Scientific) and analyzed in a continuous acetonitrile gradient consisting of 0-30% B in 240 min, 30-90% B in 3 min (B=90% acetonitrile, 0.5% acetic acid). A flow rate of ca. 200 nL/min was used to elute peptides from the RP nano-column to an emitter nanospray

needle for real time ionization and peptide fragmentation on a Q-Exactive mass spectrometer (Thermo Fisher). An enhanced FT-resolution spectrum (resolution=70000) followed by the MS/MS spectra from most intense fifteen parent ions were analyzed along the chromatographic run (272 min). Dynamic exclusion was set at 30 s. For protein identification, tandem mass spectra were extracted and charge state deconvoluted by Proteome Discoverer 1.4.0.288 (Thermo Fisher). All MS/MS samples were analyzed using SEQUESTTM (Thermo Fisher) with a fragment ion mass tolerance of 20 PPM and a parent ion tolerance of 15 PPM. Carbamidomethyl of cysteine was specified in Sequest as a fixed modification. Oxidation of methionine was specified in Sequest as a variable modification. Peptide quantification from FullScan spectra and labelling efficiency calculation were performed as described using QuiXoT, a custom software written in C#. Statistical analysis was done as reported[46]. The standardized variable Zq describes the log2 ratio for each protein corrected for the corresponding systematic error, in each experiment. Finally, data were plotted using R (v3.6.1). The code will be provided upon request. Statistical data on all proteomics analysis are presented in **Supplementary Table 8**.

Proteomic analysis of neutrophils by tandem mass tag (TMT)

For proteomic analysis of human neutrophils, two million isolated cells were pelleted in 1.5ml Eppendorf Tubes and snap-frozen at -80ºC. Upon analysis of purity, the best 5 samples (96 % mean purity) were used for multiplexed proteomic analysis at 8 am and 2 pm. For mouse neutrophils, one hundred thousand cells were sorted from Bmal1$^{\Delta N}$ mice at ZT5 or ZT13 (see cell sorting section below).

Total protein extracts from each sample were treated with 50 mM iodoacetamide (IAM) and digested overnight at 37°C with trypsin (Promega, Madison, WI, USA) at a 40:1 protein:trypsin (w/w) ratio using the Filter Aided Sample Preparation (FASP) digestion kit (Expedeon) according to manufacturer's instructions. The resulting peptides were desalted with C18 Oasis cartridges (Waters Corporation, Milford, MA, USA), using 50% acetonitrile (ACN) (v/v) in 0.1% trifluoroacetic acid (v/v) as eluent, and vacuum-dried. The peptides were TMT-labeled following manufacturer's instructions, desalted, separated into 4 fractions using the high pH reversed-phase peptide fractionation kit (Thermo Fisher) and analyzed using a Proxeon Easy nano-flow HPLC system (Thermo Fisher, Bremen, Germany) coupled via a nanoelectrospray ion source (Thermo Fisher) to a Q Exactive HF Orbitrap mass spectrometer (Thermo Fisher). C18-based reverse phase separation was used with a 2-cm trap column and a 50-cm analytical column (EASY column, Thermo Fisher) in a continuous acetonitrile gradient consisting of 0-30% A for

240 min, 50-90% B for 3 min (A= 0.1% formic acid; B= 90% acetonitrile, 0.1% formic acid) at a flow rate of 200 nL/min. Mass spectra were acquired in a data-dependent manner, with an automatic switch between MS and MS/MS using a top 15 method. MS spectra in the Orbitrap analyzer were in a mass range of 400–1500 m/z and 120,000 resolution. HCD fragmentation was performed at 28 eV of normalized collision energy and MS/MS spectra were analyzed at 30,000 resolution in the Orbitrap.

All database searches were performed with Proteome Discoverer (version 2.1, Thermo Fisher) using SEQUEST-HT (Thermo Fisher) against a Uniprot database containing all sequences from Human (July, 2018; 20,408 entries). For database searching, parameters were selected as follows: trypsin digestion with 2 maximum missed cleavage sites, precursor mass tolerance of 2 Da, fragment mass tolerance of 30 ppm. Methionine oxidation (+15.994915) was set as a variable modification. Lysine and peptide N-terminal modification of + 229.162932 Da, as well as cysteine carbamidomethylation of +57.021464 Da, were set as fixed modifications. The same MS/MS spectra collections were also searched against inverted databases constructed from the same target databases. Peptide identification from MS/MS data was performed using the probability ratio method. False discovery rates (FDR) of peptide identifications were calculated using the refined method. A 1% FDR was used as the peptide identification criterion. Each peptide was assigned only to the best protein proposed by the Proteome Discoverer algorithm.

Quantitative information from TMT reporter intensities was integrated from the spectrum level to the peptide level, and then to the protein level based on the WSPP model[58] using the Generic Integration Algorithm (GIA)[59,60]. Briefly, for the human experiment, for each sample i, the values $x_{qps} = \log_2 A_i/Ci$ were calculated, where A_i is the intensity of the TMT reporter of the 2pm sample from the individual i in the MS/MS spectrum s coming from peptide p and protein q, and Ci is the intensity of the TMT reporter from the 8am sample from the same individual. Protein quantifications where further integrated among the 5 comparisons in the human experiment, obtaining for every protein averaged value ($x_q{}'$) with their corresponding weights ($w_q{}'$)[60].

In the mouse TMT experiments, for each sample i, the values xqps= $\log_2 A_i/C_i$ were calculated, where A_i is the intensity of the TMT reporter from the individual *i* in the MS/MS spectrum *s* coming from peptide *p* and protein *q*, and C_i is the averaged intensity of the TMT reporters from all the samples in the given TMT experiment. The log2-ratio of each peptide (x_{qp}) was calculated as the weighted mean of its spectra, the protein values (x_q) were the weighted mean of its peptides, and the grand mean ($\bar{x}$) was calculated as the weighted mean of all the

protein values[58]. The statistical weights of spectra, peptides, and proteins (w_{qps}, w_{qp} and w_q, respectively) and the variances at each one of the three levels ($\sigma_{\mathbf{S}}^2$, $\sigma_{\mathbf{P}}^2$, and $\sigma_{\mathbf{Q}}^2$, respectively), were calculated as described [58]. Protein quantifications where further integrated among the corresponding replicates from the same condition, obtaining for every protein averaged values ($x_q{}'$) with their corresponding weights ($w_q{}'$) [58].

In all cases, protein abundance changes were then expressed in standardized units (Z_q), from which statistical significance of the changes in terms of the p-value were calculated. P-values were corrected for multiple hypothesis testing by controlling for the False Discovery Rate (FDR). Significant abundance changes of proteins in the compared samples were considered significant at 1% FDR.

Data were analyzed using R (v3.6.1). The analysis code will be provided upon request. Statistical data on all proteomics analysis is presented in **Supplementary Table 8**.

Proteomics-transcriptomics correlations

To analyze the correlation between proteomics and transcriptomics data of fresh and aged neutrophils, we compared our proteomics data with previously-generated RNA sequencing data on fresh (sorted at ZT13 from blood) and aged neutrophils (sorted at ZT5 from blood) available in GEO: GSE86619 [12]. To this end we obtained a set of common proteins and genes from both datasets, compared the proteomics Z-score and the sequencing Log2FC (both inform about the relative enrichment in fresh neutrophils) and calculated the regression (Spearman) statistics using R (v3.6.1). We performed similar analyses for paired transcriptome and proteome data from human samples.

Cytometry and cell sorting

Cytometric analyses were performed using a Sony SP6800 Spectral Analyzer (Sony Biotechnology, Japan). Analysis was performed using Flowjo vX (Tree Star Inc, Ashland, OR). Cell sorting experiments were performed using an FACS Aria cell sorter (BD Biosciences). All analyses were conducted at the Cellomics Unit of the CNIC. The following antibodies and streptavidin conjugates were used in this study:

Antibody /	Clone	Species	Manufacturer
CD16-APC	3G8	Human	BD
CD62L-FITC	DREG56	Human	BD
CD11b-PE	M1/70	Human/Mouse	Tonbo biosciences
Ly6G-AF647	1A8	Mouse	eBioscience

CD45-APC/Cy7	104	Mouse	Biolegend
CXCR2-PerCP-Cy5.5	SA044G4	Mouse	Biolegend
CXCR4-PE	2B11	Mouse	eBioscience
CD41-PE	MWReg30	Mouse	eBioscience
CD62L-FITC	MEL-14	Mouse	eBioscience
CD11b-BV510	M1/70	Mouse	Biolegend
CD31-APC	390	Mouse	eBioscience
CD31	2H8	Human/Mouse	Thermo Fisher
MPO-biotin	Polyclonal	Human/Mouse	R&D (biotinylated in-house)
citH3 (R2+R8+R17)	Polyclonal	Human/Mouse	Abcam
Goat-anti-hamster-AF405	Polyclonal	Hamster	Jackson ImmunoResearch
Goat-anti-rabbit-AF647	Polyclonal	Rabbit	Thermo Fisher
Streptavidin-AF488	N/A	Mouse/Human/Rat	BioLegend

In vivo NET formation during ischemia/reperfusion

The cremaster muscle was exteriorized as reported [12], and ischemia was achieved by occlusion of the inflowing and outflowing vessels by clamping the tissue connecting the muscle and the animal's body with a 15mm Micro Serrefine clamp (Fine Science Tools, Heidelberg, Germany) for 45 min. Reperfusion was achieved by removal of the clamp. 15 min after reperfusion, mice were euthanized and cremaster muscle removed for analysis. Excised muscles were fixed in 4% paraformaldehyde at 4ºC overnight and then washed 3 times in PBS containing 0.5% Triton-x 100 (PBST) and blocked for 2 h in PBST 25% FBS at room temperature with shaking. Staining was performed using anti citrunillated-H3, anti-MPO and anti-CD31 antibodies in 10% FBS-PBST overnight at 4ºC with shaking. Then, secondary antibodies were stained in 10%FBS-PBST for 4h at room temperature. Samples were then washed and mounted in Mowiol 4-88 (Mw 31,000; Sigma). Imaging of whole-mount cremaster muscles was performed using a Nikon A1R confocal system coupled to a Nikon Eclipse-Ti inverted microscope with the following lines: Diode 402nm Argon Laser 457, 476, 488, 514nm Diode 561nm HeNe Laser 642nm using a Plan Apo 10x/0,45 dry objective and the software NIS Elements AR 4.30.02 (Build 1053 LO, 64 bits, Nikon Instruments, Tokyo, Japan), and were afterwards analyzed using Imaris (Bitplane AG, Zurich, Switzerland). All imaging was performed at the Microscopy & Dynamic Imaging Unit of CNIC.

Quantification of primary granules

Blood samples were extracted every 4 h during 24 h from wild-type mice, starting at ZT1. 100 microliters of blood were RBC-lysed in hypotonic lysis buffer (0.15M KH_4Cl, 0.01M $KHCO_3$ and 0.01M EDTA in water), washed with PBS and resuspended in 40 microliters of PBS. Smears

were then performed onto Superfrost Plus microscope slides (Thermo Scientific, Waltham, USA), air-flow dried and immediately fixed in 4% PFA for 10 min at room temperature. For the experiments with mutant mice, neutrophils were sorted as described, cytospun (600 RPM, medium acceleration) into microscope slides and fixed with PFA 4% for 10 min at room temperature. For CXCL2 stimulation experiments, sorted neutrophils were plated with RPMI medium on Poly-L-lysine covered 8-well µ-Slides (Ibidi, Martinsried, Germany) and left 30 min to adhere. Cells were then incubated for 1h with 50ng/ml of recombinant CXCL2 (R&D Systems) or vehicle, and fixed with 4% PFA in PBS.

For neutrophils in blood vs tissues, we sorted cells and cytospun them as described. Prior to sorting, the tissues were extracted and kept in cold PBS (except liver, kept at room temperature in HBSS) and processed immediately after. To avoid activation of neutrophils, we did not perform digestion of the tissues, but mechanically dissociated them into single-cell suspensions by straining in 100µm pore cell strainers (Falcon). Enrichment of leukocytes from liver was performed by 36% Percoll (GE Healthcare) in HBSS (Invitrogen) gradient centrifugation. Single-cell suspensions were incubated with antibodies against CD45, CD11b and Ly6G prior to sorting of CD45+, CD11b+, Ly6G+ neutrophils. Finally, cytospun neutrophils were fixed as described above.

For the light cycle inversion experiments, WT mice were housed in light cabinets with inverted light cycle for three weeks prior to blood withdrawal for analysis. Then, whole blood extracted in EDTA tubes was RBC-lysed and smears were performed as described above.

In all cases, after washing, cells were permeabilized for 30 min with 0.1% Triton, 25% FBS in PBS and stained with biotinylated anti-MPO antibody at 4ºC overnight. Afterwards, cells were washed and incubated with A488-conjugated Streptavidin for 3h at room temperature. Finally, cells were washed, stained with DAPI and mounted in Mowiol. Imaging was performed using a Leica SP8 X confocal microscopy system coupled to a DMI6000 inverted microscope, with 100x (HC PL Apo CS2 100x/1.4 OIL) magnification objective. Granule contents were analyzed using the Imaris software.

Ex vivo NET-formation assays

Neutrophils were sorted as previously described and $5x10^4$ neutrophils were plated with RPMI medium on Poly-L-lysine covered 8-well µ-Slides (Ibidi, Martinsried, Germany), and left 30 min to adhere. Subsequently, cells were incubated for 2h with 100nM PMA or vehicle. Cells were then fixed using PFA 4% for 10 min, permeabilized with PBS 0.1% Triton X-100 1% goat serum

plus 5% BSA and stained with antibodies against citrullinated histone 3, DNA (Sytox green, Molecular Probes) and MPO. Whole-slide z-stack tilescan images were acquired with a Nikon A1R confocal system coupled to a Nikon Eclipse-Ti inverted microscope or a Leica SP5 confocal microscope and analysed using Imaris.

Antibody-induced acute lung injury (ALI)

A two-event model of transfusion-related ALI was adopted for our studies as described [15]. Male Balb/c mice (7-14 week-old) were injected intraperitoneally with 0.1 mg/kg LPS. 24 hours later, mice received an intravenous injection of 0.5 mg/kg anti-H2d (clone 34-1-2s; BioXcell) antibody. Some mice were treated 1h before ALI induction with 12mg/kg of Cl-Amidine (Cayman Chemical Company, Ann Arbor, Michigan, USA) to block NET-formation (31). For survival experiments, mice were observed for 2h during the acute phase of ALI.

Neutrophil elastase activity assay

NE activity in plasma was measured using a commercially available kit (Neutrophil Elastase activity assay kit - Fluorometric, NAK246-1KT, Sigma-Aldrich) according to the manufacturer's instructions. We analyzed 50 microliters of plasma, with an excitation wavelength of 390nm and emission wavelength of 510nm in a Fluoroskan Ascent plate reader (Thermo Labsystems). Standard curve goodness of fit had an R-square of 0.99 in linear regression.

Intravital imaging of the lung

Intravital microscopy of the lung was performed as reported [28]. Briefly, mice were anesthetized and mechanically ventilated through the trachea using a small animal ventilator model 687 (Harvard Apparatus). Then, right lateral thoracotomy was applied, and the lung was positioned under the window of a custom-built fixation device. A mil vacuum was applied to hold the lung in position during microscopy. Mice were injected with AF647-conjugated Ly6G antibody to stain neutrophils, PE-conjugated CD41 antibody to stain platelets and Sytox green (Molecular Probes) to stain extracellular DNA. 4D imaging was performed for each mouse in 5 random fields inside the visualization window, using the VIVO system[12]. Analysis was performed in Imaris software. For NET-like structures, we quantified the number of spots in the neutrophil-extracellular DNA colocalization channel over time in all random fields.

Analysis of NET types in lungs

We found two types of NET-formation events in lungs during ALI. Flowing NETs were defined as events in which DNA was rapidly extruded out of the neutrophil and most commonly was washed away by the flow; and adherent NETs, which were defined as DNA being deployed

slowly around the uropod region of the neutrophil as it crawled, stuck to the vasculature and was more resistant to blood-flow washing. To quantify the relative frequency of each of them, we visually inspected every NET formation event in our time-lapse footage and ascribed each event to one of the two categories, or none if it was unclear.

Whole mount immunostaining and tissue clearing

To confirm the presence and abundance of NETs in the lungs of mice upon ALI induction we performed whole mount immunostaining and tissue clearing of excised lungs. Mice were subject to ALI and euthanized with CO_2 15 min after ALI induction. Mice were then perfused with 20ml of saline through the left ventricle of the heart, and the lungs were collected in cold PBS. Afterwards, lungs were fixed at 4ºC overnight in PBS with 4% PFA and 30% sucrose. After 3 washes of 1h with PBS at room temperature, tissues were permeabilized in methanol gradients in PBS for 30 min (PBS > MetOH 50% > MetOH 80% > MetOH 100%). Then, tissues were bleached with Dent's bleach (15% H_2O_2, 16.7% DMSO in MetOH) for 1h at room temperature, and then were rehydrated through descending methanol gradients in PBS (MetOH 80% > MetOH 50% > PBS). Then tissues were incubated with blocking buffer containing PBS with 0.3% Triton X100, 0.2% BSA, 5% DMSO, 0.1% azide and 25% FBS overnight at 4ºC with shaking. Afterwards lungs were stained with antibodies against citrunillated histone 3, MPO and CD31 for 2 days at 4ºC with shaking. After washing for 24h in washing buffer (PBS with 0.2% Triton X100 and 3% NaCl), the tissues were stained with secondary antibodies anti-rabbit AF647, antiHamster-AF405 and Streptavidin AF488 for 24h at 4ºC with shaking. 24h later, tissues were washed for 24h in washing buffer and were dehydrated in MetOH gradients in dH_20 using glass containers for 30 min in each step (MetOH 50% > MetOH 70% > MetOH 90% > 3x MetOH 100%). Finally, tissues were cleared for 30 min in MetOH with 50% BABB and afterwards in 100% BABB (benzyl alcohol, benzyl benzoate 1:2) and imaged in a Leica SP8 X confocal microscopy system coupled to a DMI6000 inverted microscope.

Computerized tomography (CT) for in vivo edema quantification

In vivo CT imaging was performed on a nanoPET/CT small-animal imaging system (Bioscan, Washington DC) equipped with a micro-focus X-ray source and a high-resolution detector (1024x3596 pixels; 48 μm pixel size). Acquisition parameters were 55 kVp and 73 μAs. Mice were intraperitoneally anesthetized and positioned onto a thermoregulated (30 degrees) mouse bed until the scan was completed. An ophthalmic gel was administered in their eyes to prevent retinal drying. Six studies were acquired per animal: one prior the retro-orbital injection of anti-H2d to induce ALI, and five post-injection during 30 min approximately. Data were acquired in

helical mode obtaining 240 projections per rotation with 768 µm pixel size. Reconstruction was performed with an FDK-based method included in the proprietary Nucline software (Mediso, Budapest, Hungary). Pulmonary edema was quantified using Horos software (The Horos Project, distributed under the LGPL license at Horosproject.org and sponsored by Nimble Co LLC d/b/a Purview in Annapolis, MD, USA) as the change of the mean value, in Hounsfield Units, within the region of interest of the lungs obtained by thresholding (-1000 and -400 lower and upper thresholds, respectively) followed by a closing morphological operation.

Intravital imaging of the cremaster muscle to quantify platelet-neutrophil interactions

Intravital microscopy of the cremaster muscle after TNFα stimulation (R&D Systems, 0.5µg intrascrotal injection) was performed as previously reported [12, 15] using the VIVO system. Ten to twenty venules segments per mouse were analyzed 150 to 210 min after TNF-α treatment in multiple fluorescence channels (Cy3/561 for PE, FITC/488 for FITC and Cy5/640 for APC) and bright-field images with 1x1 or 2×2 binning with 3 second interval for 2 min on each field of view. For double staining with PE- and FITC-conjugated antibodies, acquisition was facilitated in single (FITC) and quadrant (PE) filters in order to avoid bleed-through of fluorescent signals between channels. For the visualization of leukocytes, fluorescently labelled anti-Ly6G-APC and anti-CD62L-FITC antibodies were injected, and to visualize platelets, anti-CD41-PE was injected intravenously at 1 µg/mouse. Quantification of neutrophil-platelet interactions in either the leading edge or trailing edge was performed using Slidebook (3I).

Circadian analysis of neutrophil phenotypes

Circadian blood samples were extracted every 4 h during 24 h from wild-type or experimental mice, starting at ZT1 (Zeitgeber time, 1 hour after the onset of light, 7:00 at the CNIC's animal facility). For circadian surface marker analysis, blood counts were analyzed in an automated hemocytometer (Abacus Junior, Diatron; Holliston, USA), RBC were lysed in hypotonic lysis buffer (0.15M KH4Cl, 0.01M KHCO3 and 0.01M EDTA in water) and incubated 15 min with 0.25 µg anti-Ly6G, -CD62L and -CXCR2 antibodies, washed and analysed in a Sony SP6800 Spectral Analyzer. Analysis was performed using Flowjo vX (Tree Star Inc, Ashland, OR).

Vascular permeability assay

A 0.5% solution of Evans blue in sterile PBS was prepared and 200µl of the solution was i.v. injected into mice 15 min before TRALI induction (or just LPS injection as control, see protocol for ALI). 15 min later mice were sacrificed, and tissues extracted and weighted. Then, tissues were submerged in 0.5 ml formamide and incubated at 55ºC for 24h. Tissues were removed,

and the tubes centrifuged for 5 min at 645 g. Finally, supernatants were measured for absorbance at 610nm using an xMark Microplate Spectrophotometer (BioRad) plate reader.

Human studies

We performed human proteomics, RNA sequencing, NET-formation assays and granule quantification (see individual methods) in neutrophils from blood samples of heathy volunteers obtained at 8am, 2pm and 7pm at Hospital 12 de Octubre. The study complied with all ethical regulations and was approved by the Ethical Research Committee of Hospital 12 de Octubre in Madrid (CEIm #18/389), and informed consent was obtained from all volunteers.

Human neutrophil granule quantification

Diurnal blood samples were extracted from healthy volunteers at 8am, 2pm and 7pm. One hundred microliters of blood were processed as imaged as indicated above for mouse neutrophils.

Human neutrophil isolation

12 ml of freshly obtained blood extracted from healthy volunteers at the indicated times were used to isolate human neutrophils using Histopaque 1119 and 1077 (Sigma) gradients. In a 50ml falcon tube 15ml of Histopaque 1119 were added and then 15 ml of Histopaque 1077 were carefully layered on top. Whole blood was carefully layered on top of the low-density solution, and tubes were centrifuged for 30 min at 340g at room temperature, with no brakes or acceleration. Neutrophils layering between the 1077 and 1119 interphase were carefully aspirated and the isolated neutrophils washed twice in PBS. We obtained over 95% purity as assessed by flow cytometry.

RNA sequencing of human neutrophils

Total RNA was prepared with the RNA Extraction RNeasy Plus Mini-kit (QIAGEN). 1 ng of total RNA were used to generate barcoded RNA-seq libraries as previously described[12].

Libraries were sequenced on a HiSeq2500 (Illumina) to generate 60 bases single reads. FastQ files for each sample were obtained using *bcl2fastq* 2.20 Software software (Illumina). The RNA sequencing experiments were performed at the Genomics Unit at CNIC.

Human ex vivo NET formation assay

$4x10^4$ Human neutrophils isolated as previously described were plated with RPMI medium on Poly-L-lysine covered 8-well µ-Slides (Ibidi, Martinsried, Germany) and left 30 min to adhere.

Adherent cells were incubated for 2h with 250ng/ml PMA or vehicle and then fixed using PFA 4% for 10 min, permeabilized with PBS 0.1% Triton X-100 1% goat serum plus 5% BSA and stained with antibodies against citrullinated histone 3 (Abcam, Cambridge, UK), DNA (Sytox green, Molecular Probes) and MPO (R&D Systems). Whole-slide z-stack tilescan images were acquired with a Leica SP5 confocal microscope. Analysis of extra-nuclear DNA was performed using ImageJ with an automated method for extranuclear DNA quantification made available in https://doi.org/10.6084/m9.figshare.7358642.v1

Retrospective analysis of human ARDS

Data from acute respiratory distress syndrome (ARDS) was extracted from a prospective observational cohort study of 5334 consecutive adult patients with community-acquired pneumonia admitted to the ICU that developed ARDS between 1996 and 2016 [32], in Hospital Clinic of Barcelona, Spain. The time of admission, severity and survival was determined for the 125 patients that developed ARDS. Patients were excluded if they had severe immunosuppression or active tuberculosis. ARDS was identified based on the Berlin definition. Only time points with 3 or more data points were included in subsequent analysis. The study was approved by the ethics committee of Hospital Clinic of Barcelona (no. 2009/5451).

Transmission electron microscopy imaging of neutrophils

Neutrophils from mouse and human blood were isolated as previously described (FACS sorting for mouse neutrophils, gradient isolation for human neutrophils), fixed in 4% PFA for 10 min and washed with PBS. Samples were then post-fixed in distilled water containing 4% of osmium tetroxide for 1h at room temperature. After washing in distilled water, samples were stained in a block with uranyl acetate 0.5% in water for 10 min. Then, samples were dehydrated in ascending gradients of ethanol in water (30%, 50%, 70%, 95% and 100%) with a last step in acetone. Samples were then included in epoxi resin (Durcupan) in ascending steps of resin:acetone (1:3, 3:1) and then pure resin. Samples included in the resin were polymerized for 48h at 60ºC and 60nm slices were obtained in a Leica Ultracut S ultramicrotome in 200 mesh Cu gratings. Finally, samples were counterstained with uranyl acetate and lead citrate. Images were acquired in a 100Kv Jeol JEM1010 TEM microscope (Tokyo) with a Gatan SC200 (Pleasanton CA) camera coupled to the system. Quantification of granule-covered cytoplasmic area was performed in ImageJ using a custom-made macro that allows calculation of cell, nucleus and granule areas, made available in: https://doi.org/10.6084/m9.figshare.7619093.v1

Code availability

ImageJ macros for TEM granule quantification and extracellular DNA quantification are available in FigShare (see the relevant method for specific links). All other pieces of code are available upon request.

Statistical analysis

Unless otherwise indicated, data are represented as mean values ± standard error of the mean (SEM). Paired or unpaired two-tailed t-test was used when 2 groups were compared, and comparison of more than two data sets was done using one-way analysis of variance (ANOVA) with Turkey's post-test. Where applicable, normality was estimated using D'Agostino & Pearson or Shapiro-Wilk normality test. Log-rank analysis was used for Kaplan-Meier survival curves. Sample exclusion was not performed unless evident signs of disease were found in a mouse. For determination of diurnal patterns, we performed COSINOR fitting of circadian curves [12]. To determine whether a diurnal curve displayed an oscillating pattern we used the COSINOR-calculated amplitudes and compared them with a hypothetical zero-amplitude curve (i.e. with no circadian behavior) assuming that both curves have identical standard deviations. We finally compared the two curves' amplitudes using unpaired two-tailed t-test analyses. All statistical analyses were performed using Prism v7 (GraphPad Software, California, USA), except proteomics and sequencing analysis, which were performed using R (see individual methods). A p-value below 0.05 was considered statistically significant; non-significant differences (n.s.) are indicated accordingly.

Data availability

Proteomics data for mouse and human neutrophils are available in the Peptide Atlas with accession number: PASS01364. Proteomics data for Bmal1$^{\Delta N}$ mice at ZT5 and ZT13 and WT vehicle vs AMD-3100 treated mice are also available in the Peptide Atlas with the accession number: PASS01438. Mouse circadian transcriptomics used for the correlation analysis are available at the Gene Expression Omnibus with accession number GSE102310. Human sequencing data used for the correlation analysis are available at GEO with accession number: GSE136632. All other pieces of data are available upon request.

References for methods

45. Navarro P, Trevisan-Herraz M, Bonzon-Kulichenko E, Nunez E, Martinez-Acedo P, Perez-Hernandez D*, et al.* General statistical framework for quantitative proteomics by stable isotope labeling. *J Proteome Res* 2014, **13**(3)**:** 1234-1247.

46. Garcia-Marques F, Trevisan-Herraz M, Martinez-Martinez S, Camafeita E, Jorge I, Lopez JA*, et al.* A Novel Systems-Biology Algorithm for the Analysis of Coordinated Protein Responses Using Quantitative Proteomics. *Mol Cell Proteomics* 2016, **15**(5)**:** 1740-1760.

47. Trevisan-Herraz M, Bagwan N, Garcia-Marques F, Rodriguez JM, Jorge I, Ezkurdia I*, et al.* SanXoT: a modular and versatile package for the quantitative analysis of high-throughput proteomics experiments. *Bioinformatics* 2019, **35**(9)**:** 1594-1596.

Figures and Figure legends

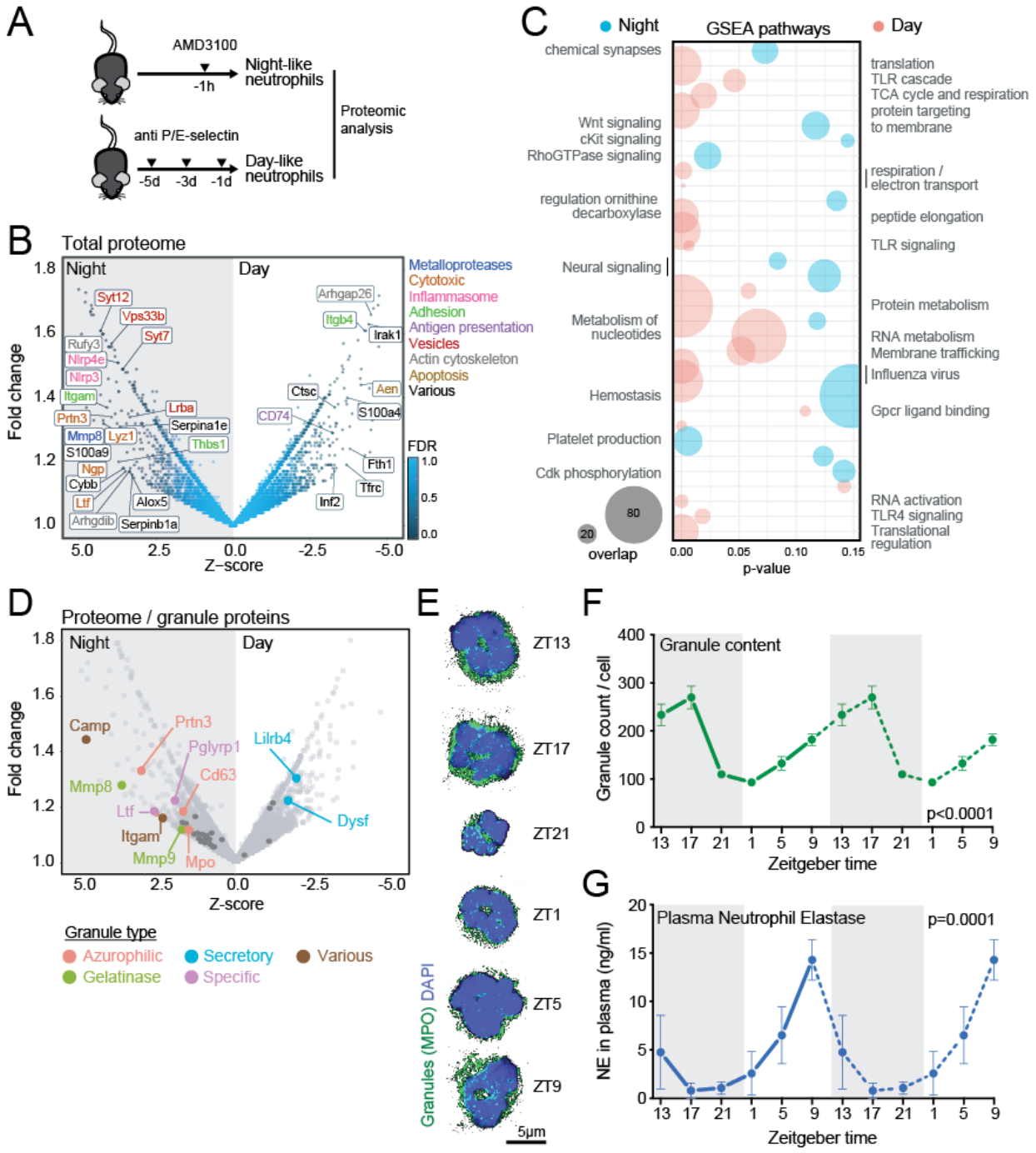

Figure 1. Diurnal changes in the neutrophil proteome.
(A) Experimental strategy for proteomic analysis of aged and fresh neutrophils. (B) Volcano plot of proteins with a False Discovery Rate (FDR) < 0.01. A positive Z-score represents an increase in nighttime (fresh) over daytime (aged) neutrophils. Color represents the functional category for each protein (legend, top-right). (C) Gene-set enrichment analysis of the proteomics data showing

pathways with a p-value < 0.15 enriched in aged (red) or fresh (blue) neutrophils. Size of the bubble-plot represents overlap between query and gene-set (legend bottom-right). (D) Volcano plot of the proteomic dataset showing granule proteins with a Z-score > 2. Colors show the granule type for each protein. (E) Z-stack maximum projection of neutrophils stained for primary granules with MPO and counterstained with DAPI. (F) Quantification of neutrophil granule contents during a full diurnal cycle. Curves are repeated (dashed line) to better appreciate the circadian pattern. Dark phase is shown in grey; n=30 cells per time point. G) Neutrophil elastase activity in plasma. Curves are repeated (dashed line) to better appreciate the circadian pattern. Dark phase is shown in grey; n=4 mice per time point. Data in (F, G) are shown as mean ± SEM, and p-values were determined by amplitude vs. zero t-test analysis (see Methods).

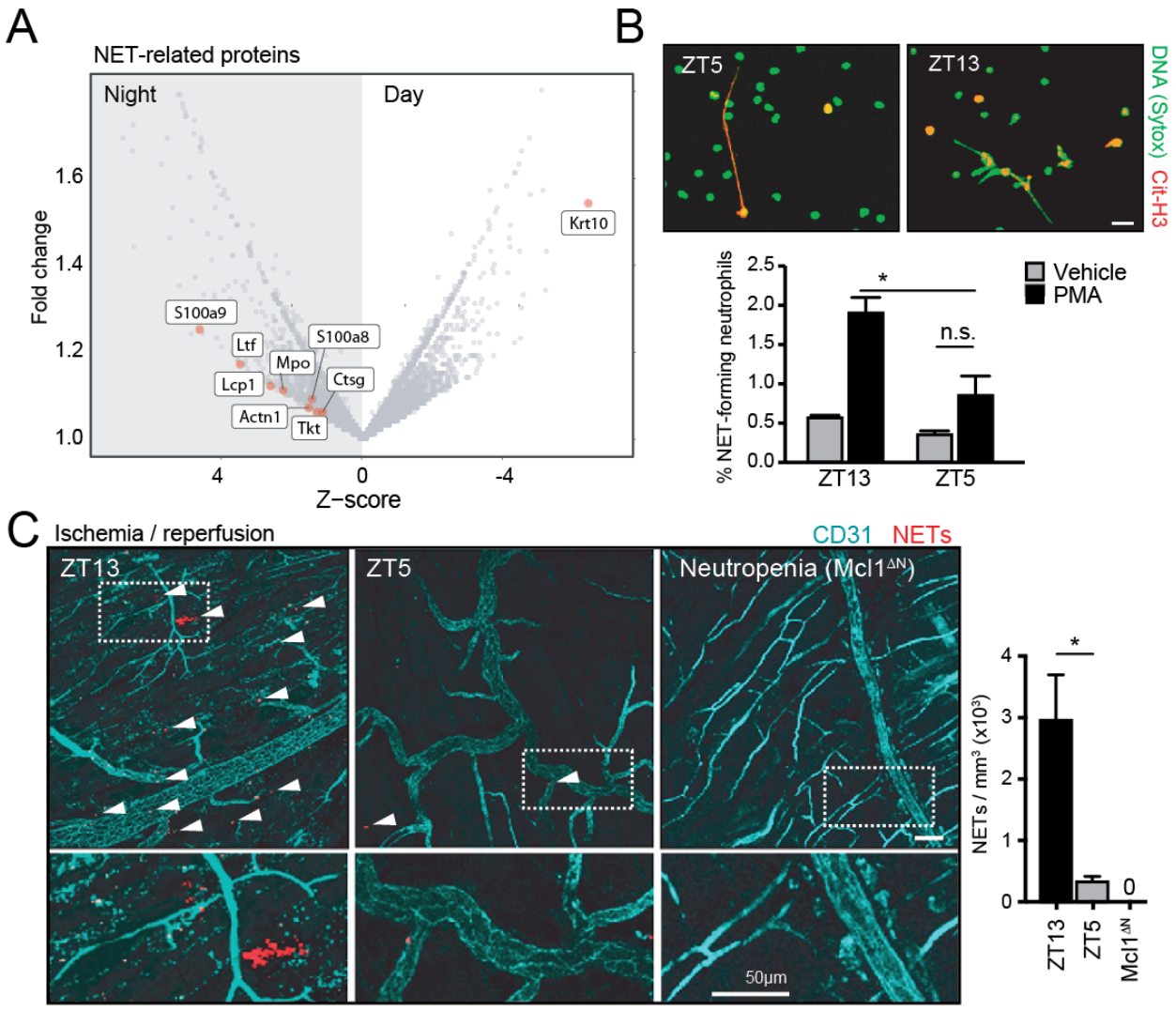

Figure 2. Diurnal loss of NET-forming capacity.

(A) Volcano plot of the neutrophil proteome showing proteins found in NETs (red dots), and enrichment of these proteins in nighttime neutrophils. (B) *Ex vivo* NET-formation assay. Neutrophils sorted at ZT13 (nighttime) or ZT5 (daytime) were stimulated with PMA or vehicle to induce NETs and stained for citrunillated-histone 3 (Cit-H3) and DNA (top). Colocalization of both markers was used to quantify NET formation as shown in the bar graph (bottom); n=3 mice per time point. (C) Representative images (left) and quantification (right) of in vivo NET formation in the cremaster muscle subjected to ischemia/reperfusion at nighttime (ZT13), or at daytime (ZT5). Triple colocalization of MPO, DNA and Cit-H3 was used to define and quantify the area of NETs (red; arrowheads). Neutropenic Mcl1$^{\Delta N}$ mice (Lyz2^{Cre}; Mcl1$^{fl/fl}$ mice) were used as controls and showed no NETs. Dotted areas are showed magnified in bottom panels; n = 3 mice per condition. Scale bars, 50 µm. Bars show mean ± SEM. *; p<0.05; n.s., not significant, as determined by unpaired t-test analysis.

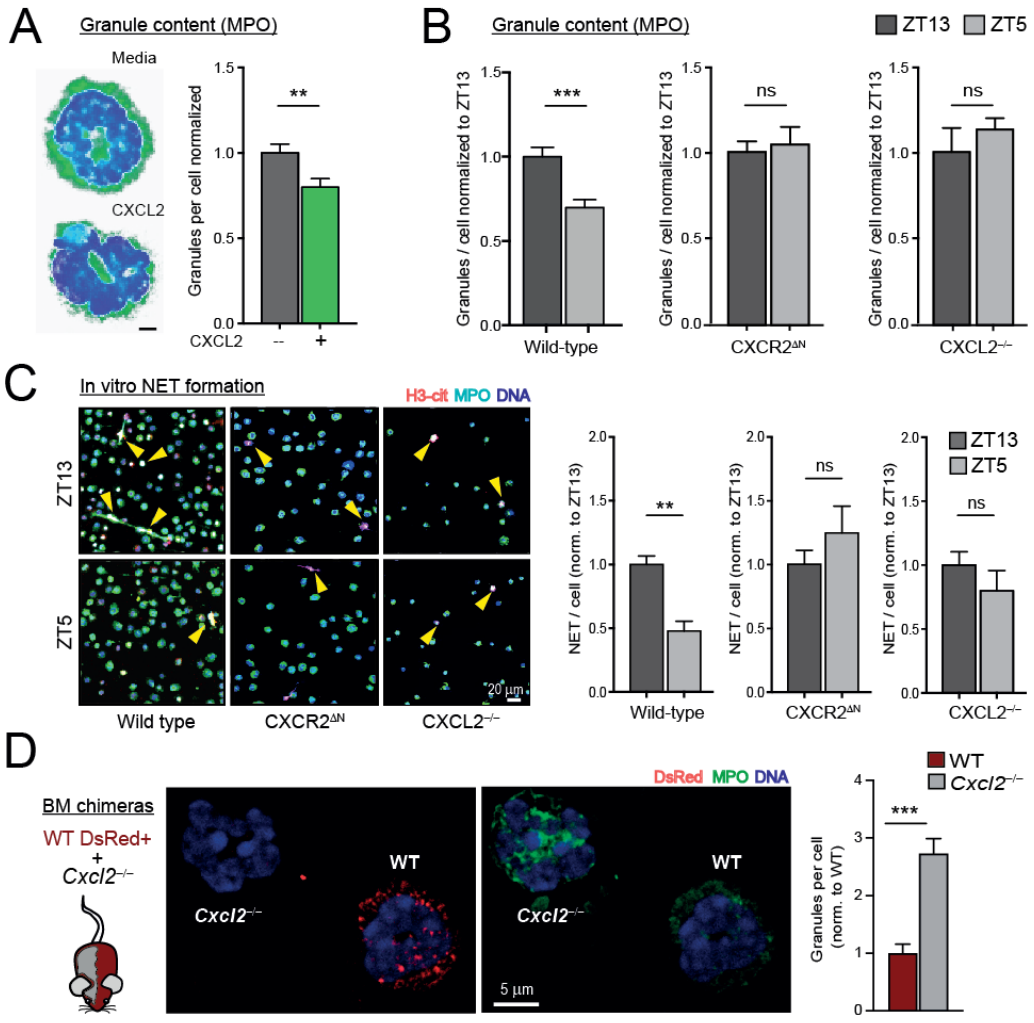

Figure 3. Degranulation and loss of NET-forming capacity are driven by CXCL2/CXCR2 signaling.

(A) Ex-vivo stimulation of sorted neutrophils with CXCL2 induces degranulation (right), as quantified by confocal imaging of MPO-stained neutrophils (left); n = 29-32 cells. (B) Diurnal quantification of granule content in neutrophils from WT, CXCR2$^{\Delta N}$ or CXCL2$^{-/-}$ mice, showing a loss of diurnal fluctuation in CXCR2-defici

ent (n = 38-40 cells) or CXCL2-deficient neutrophils (n = 15-31), compared to their WT counterparts (n = 30-33 cells per time point). (C) Ex-vivo NET formation assays with sorted neutrophils stimulated with PMA or vehicle control, at nighttime (ZT13) or daytime (ZT5). NETs were quantified by triple-colocalization of citrunillated-histone 3, DNA and MPO in confocal micrographs (left). Each mouse was normalized to its vehicle control and NET formation at ZT13 and ZT5 compared (right). CXCL2-deficient (n = 3 mice per time) and CXCR2-deficient (n = 2-6 mice per time) neutrophils showed loss of diurnal fluctuation in NET formation compared with WT cells (n = 4-6 mice per time). (D) CXCL2 signaling causes degranulation cell-autonomously, as shown by analysis of MPO+ granules in neutrophils from BM chimeras reconstituted with DsRed+ wild-type and DsRed^{NEG} *Cxcl2*$^{-/-}$ donors; n = 3 mice. Bars show mean ± SEM. **; p<0.01; n.s., not significant, as determined by paired (A) or unpaired (B-C) t-test analysis.

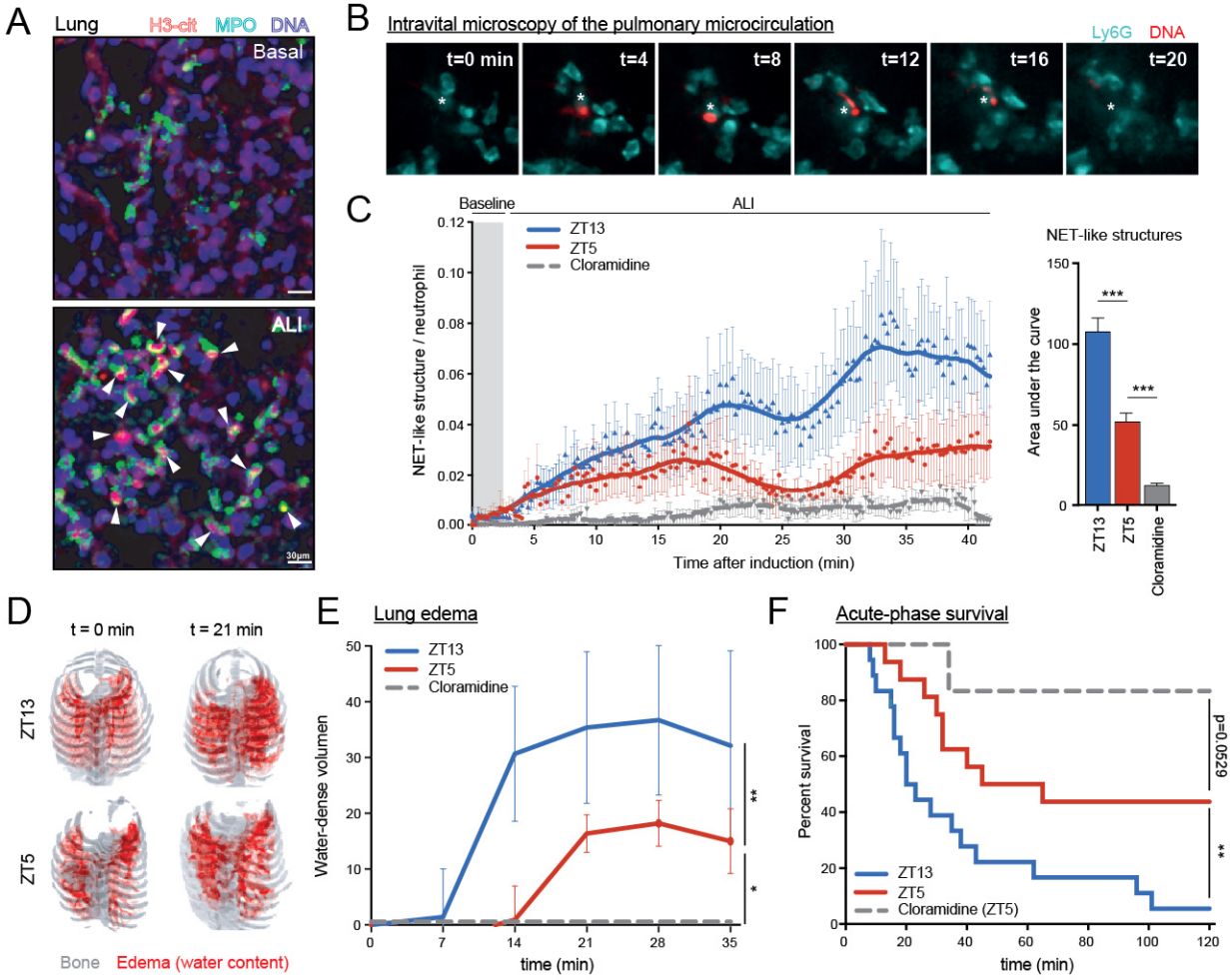

Figure 4. Diurnal loss of NET formation and pulmonary protection during ALI.
(A) Presence of NETs in lungs. Shown are maximum projections of confocal Z-stack series of cleared lungs from control mice (Basal) or mice with antibody-induced acute lung injury induction (ALI). Lungs were stained against citrunillated-histone 3, MPO and DNA, and some NETs are shown (arrowheads). (B) Time-series of 4D intravital imaging captures of NET-like structures in the lungs of ALI-induced mice. NET-like structures were defined as free DNA extruded out of Ly6G+ neutrophils. See also **Movie S1.** (C) Quantification of NET-like structures as shown in (B), and normalized to the number of neutrophils in mice in which ALI was performed at nighttime (ZT13) or daytime (ZT5), or in mice treated with Cl-amidine (at ZT5). Time course (left panel) and area under the curve values (right panel); n = 15 fields from 4 mice per condition. (D) Representative images of longitudinal CT series of edema formation at 0 or 21 min after inducing ALI ZT13 or ZT5. Note the increased edema (red) at night. Background bone signal (grey) is shown for anatomical positioning. (E) Quantification of the images in (D). Volume of edema was increased at ZT13 (blue; n = 7) relative to ZT5 (red; n = 7). Mice treated with Cl-amidine are shown as a control (grey, n = 4). (F) Survival of mice subjected to ALI at ZT13 (blue) or ZT5 (red), or treated with Cl-amidine (gray); n = 11-21 mice. Data are shown as mean ± SEM. **; p<0.01; ***, p<0.001, as determined by one-way ANOVA with Dunnet's multiple comparison test (C), two-way ANOVA (E) or log rank (Mantel-Cox) test (F).

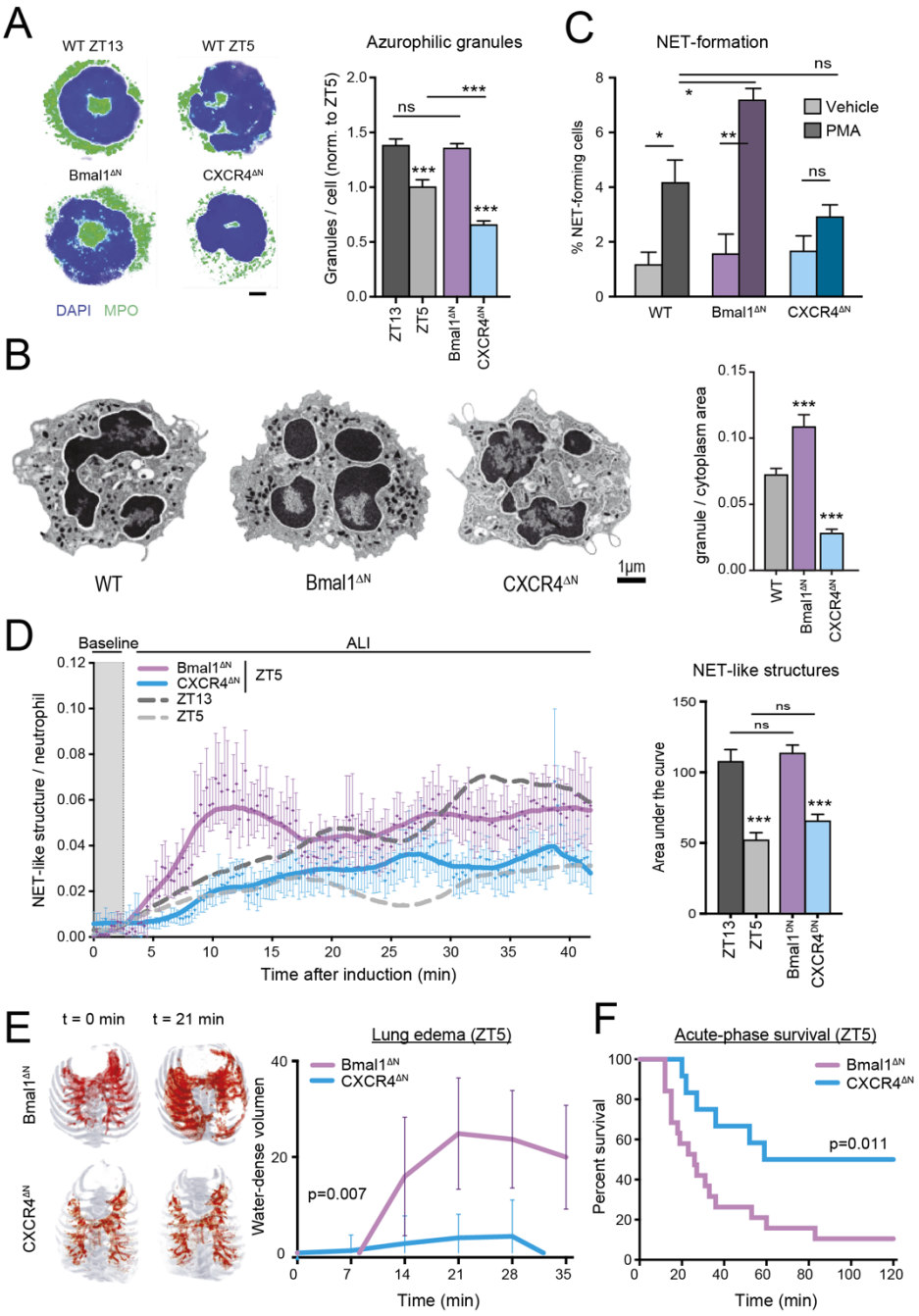

Figure 5. Diurnal degranulation and pulmonary protection is neutrophil-intrinsic.
(A) Confocal micrographs and quantification of primary granules in neutrophils from WT mice at night (ZT13) or daytime (ZT5), and from mutant mice (both at ZT5); n = 30-50 cells from 3 mice. (B) Transmission electron microscopy images (left), and quantification of electrodense azurophilic granules (right) in WT and mutant mice (all at ZT5), showing increased granule content in Bmal1$^{\Delta N}$, and reduced in CXCR4$^{\Delta N}$ neutrophils compared with WT cells; n = 19. (C) *Ex vivo* NET formation in sorted WT, Bmal1$^{\Delta N}$ or CXCR4$^{\Delta N}$ neutrophils stimulated with PMA or vehicle as control; n = 3 per condition. (D) Quantification of NET-like structures normalized to the number of

neutrophils during ALI in Bmal1$^{\Delta N}$ or CXCR4$^{\Delta N}$ mice. Time course and elevations from baseline (gray area) are shown in the left panel, and the areas under the curve are shown in the right panel. Experiments were performed at ZT5. Data from wild-type mice at ZT5 and ZT13 (from **Figure 4C**) are shown for reference; n = 15 fields from 3 mice per condition. (E) Representative images of longitudinal CT series of edema (red) in mutant mice subject to ALI (left), and quantification of the edema volume over time (right panel); n = 7 mice per genotype. (F) Survival curves of Bmal1$^{\Delta N}$ and CXCR4$^{\Delta N}$ mice subjected to ALI; n = 12-19 mice per genotype. Data are shown as mean ± SEM. *; $p<0.05$; **, $p<0.01$; ***, $p<0.001$; n.s., not significant, as determined by one-way ANOVA with Dunnet's multiple comparison test (A-D), two-way ANOVA (E) or log rank (Mantel-Cox) test (F).

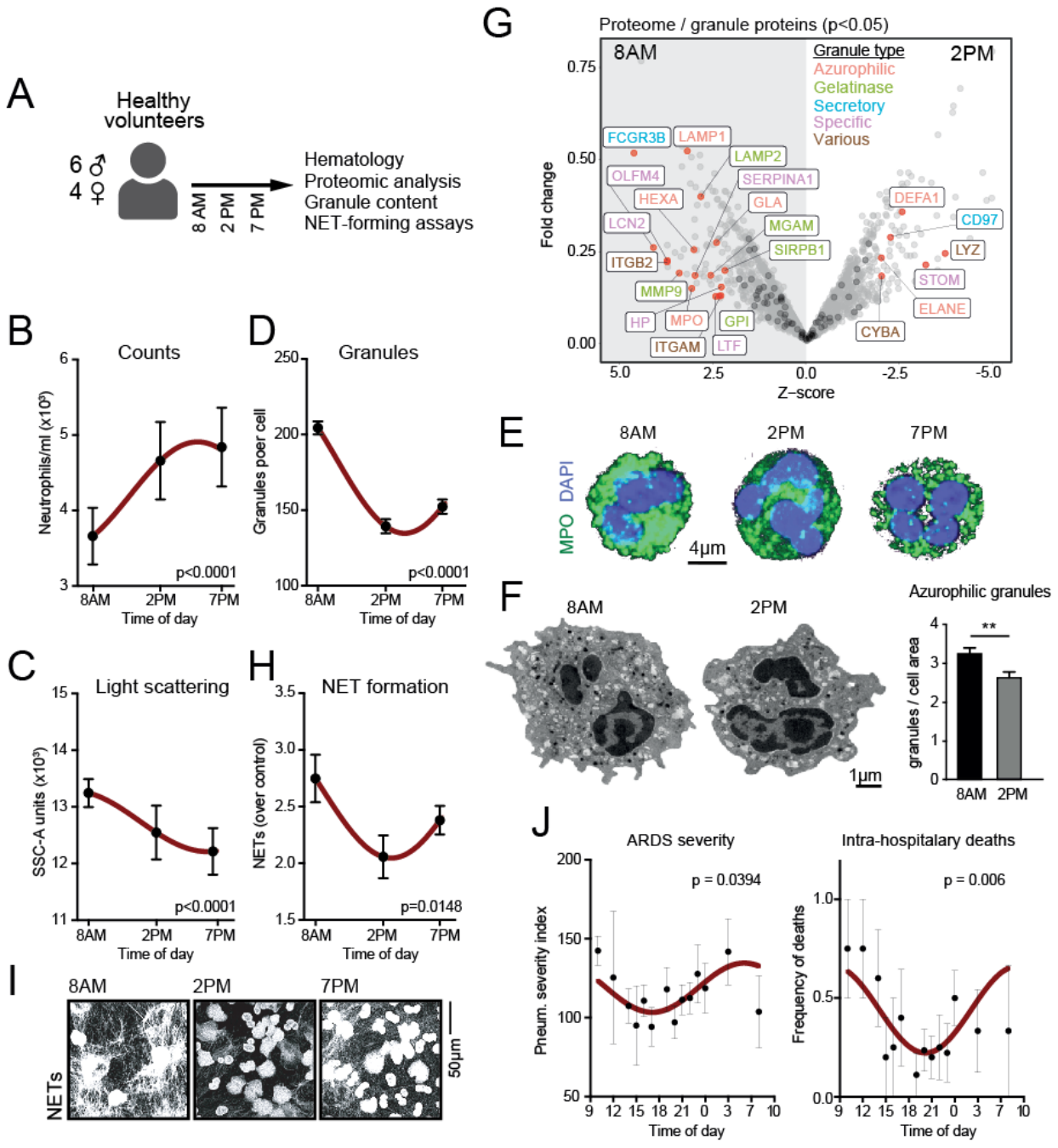

Figure 6. Evidence for neutrophil disarming and pulmonary protection in humans.
(A) Experimental design. Blood from 10 healthy volunteers was extracted at 8 am, 2pm and 7 pm. Neutrophils were purified for proteomic analysis, granule quantification and NET-formation assays. (B) Blood neutrophil counts in human volunteers at the different time points; n = 10. (C) Light scattering (SSC-A) values for human neutrophils at different times, as measured by flow cytometry; n = 10 human volunteers. (D) Quantification of primary granules from confocal images of human neutrophils from images in (E); n = 150 cells from 10 volunteers. (E) Representative images of granule content of human neutrophils. (F) Transmission electron micrographs (left) of

human neutrophils in the morning (8 am) and early afternoon (2 pm) showing reduced numbers of electrodense primary granules (right); n = 33 cells from 3 human volunteers. (G) Volcano plot of granule proteins in the human neutrophil proteome, showing higher content in granule proteins (color-coded) at 8 am compared with 2 pm; n = 5 samples from healthy volunteers. Red dots and labels show differentially expressed proteins with p-value<0.05, and black dots show all granule proteins. Label color indicates the granule type in which the protein is normally found (bottom right). (H) Quantification of *ex vivo* NET formation by human neutrophils stimulated with PMA or vehicle at the indicated time points. Representative confocal images of the PMA-induced NETs are shown in (I); n = 10 volunteers. (J) Acute respiratory distress syndrome (ARDS) severity shown as the pneumonia severity index (left) and intra-hospitalary deaths (right), of patients entering the ICU at different times of the day; n = 125 patients. Data are shown as mean ± SEM. **; p<0.01, as determined by unpaired t-test analysis (F). P values for the circadian plots were calculated by the amplitude vs. zero t-test analysis (B-D, H, J).

Extended data figures for

Programmed “disarming” of the neutrophil proteome reduces the magnitude of inflammation

Jose M. Adrover, Alejandra Aroca-Crevillén, Georgiana Crainiciuc, Fernando Ostos, Yeny Rojas-Vega, Andrea Rubio-Ponce, Catia Cilloniz, Elena Bonzón-Kulichenko, Enrique Calvo, Daniel Rico, María A. Moro, Christian Weber, Ignacio Lizasoain, Antoni Torres, Jesús Ruiz-Cabello, Jesús Vázquez and Andrés Hidalgo

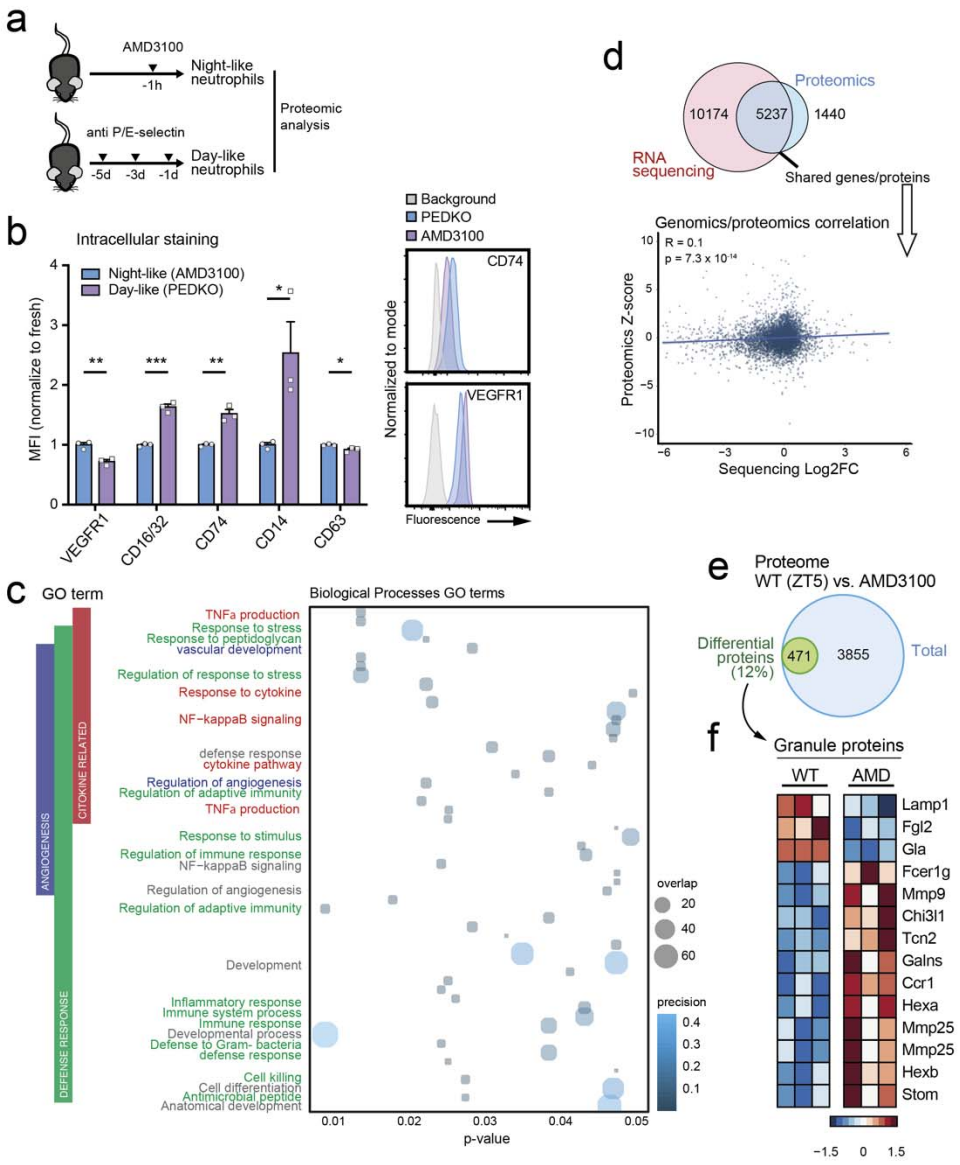

Extended Data Figure 1. Validation and analysis of neutrophil proteomics.

a, Experimental strategy for proteomic analysis of day-like (from P- and E-selectin treated mice) and night-like (from AMD3100-treated mice) neutrophils isolated by negative selection (see methods) from blood. **b**, Intracellular staining of proteins from the proteomics dataset for validation in fresh (blue) and aged (violet) neutrophils obtained as indicated in a. All the proteins analyzed correlated with the proteomics data; n=3 mice per condition. **c**, GO terms of the differentially expressed proteins (FDR < 0.05, see methods section for ^{18}O proteomics) in the proteomics dataset, showing terms with p < 0.05 (from single samples of 60 million neutrophils pooled from 9 mice (night) and 6 mice (day)). Bubble size represents overlap of query vs. the GO term. **d**, Scatterplot, correlation coefficient and significance level (pvalue) of the Spearman's correlation of the direction of change of common proteins and genes from our proteomic analysis of fresh and aged neutrophils (this paper) and circadian RNA-sequencing data previously reported (Adrover et al. 2019, from 3 mice at ZT5 and 3 mice at ZT13), showing poor correlation of RNA and protein

content. **e**, Venn-diagram showing the number of differentially detected proteins ($p<0.05$, see methods section for mouse TMT proteomics) between vehicle- and AMD3100-treated mice (at ZT5); n=3 samples per group. **f**, Heatmap showing levels of granule proteins in this dataset, Note increased detection of most granule proteins in neutrophils from AMD3100-treated mice. Data in (b) are shown as mean ± SEM. *; $p<0.05$; **, $p<0.01$; ***, $p<0.001$, as determined by unpaired two-tailed t-test analysis.

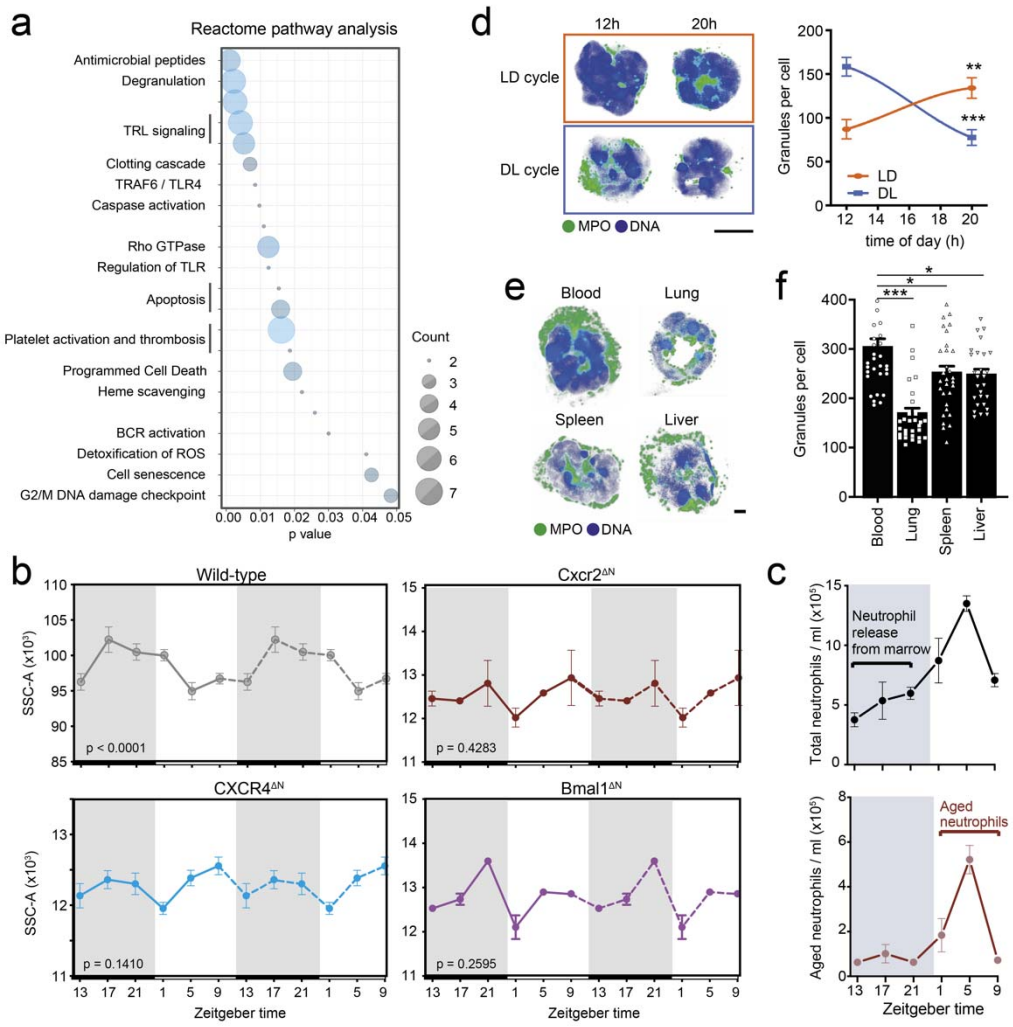

Extended Data Figure 2. Degranulation of neutrophils in the circulation and in tissues.
a, Reactome pathway analysis of the proteome of night and day neutrophils (see methods section for ^{18}O proteomics, from single samples of 60 million neutrophils pooled from 9 mice (night) and 6 mice (day)) showing pathways with p-value < 0.05. **b**, Light scattering properties (a measure of granularity) of blood neutrophils during a full diurnal cycle, measured as side-scatter in flow cytometry. Data are for WT, CXCR2-, CXCR4- or Bmal1-deficient neutrophils, showing that cell-intrinsic disruption of clock regulators blunts diurnal fluctuation in granularity. Curves are repeated for two cycles (dashed line) to better appreciate the circadian pattern; n = 10 (WT), 3 ($CXCR2^{\Delta N}$), 4 ($CXCR4^{\Delta N}$) and 4 ($Bmal1^{\Delta N}$) mice per time point. **c**, Kinetics of total (top) or aged (bottom) neutrophils in blood indicating times of release of young or accumulation of aged neutrophils; n = 5 mice (ZT13, ZT17, ZT21, ZT1 and ZT9), n = 4 mice (ZT5). **d**, Shift of the light cycle alters the pattern of granule content in neutrophils. Left, representative confocal images of sorted neutrophils (MPO, green; DAPI, blue; scale, 5 μm); right, granule content per cell at the indicated times and light regime; n=3 mice. LD, light-dark cycle; DL, dark-light (inverted) cycle. **e**, Representative confocal images (scale, 1 μm) and **f**, quantification of granule content in neutrophils from the blood or tissues of WT mice, showing reduced granule counts in tissues

compared with blood; n = 30 (blood, lung and spleen), n = 27 (Liver) cells from 3 mice. Data are shown as mean ± SEM. *; $p<0.05$; ***, $p<0.001$; n.s., not significant, as determined by one-way ANOVA with Dunnet's multiple comparison test (d), or using the amplitude vs. zero two-tailed t-test for circadian curves (b).

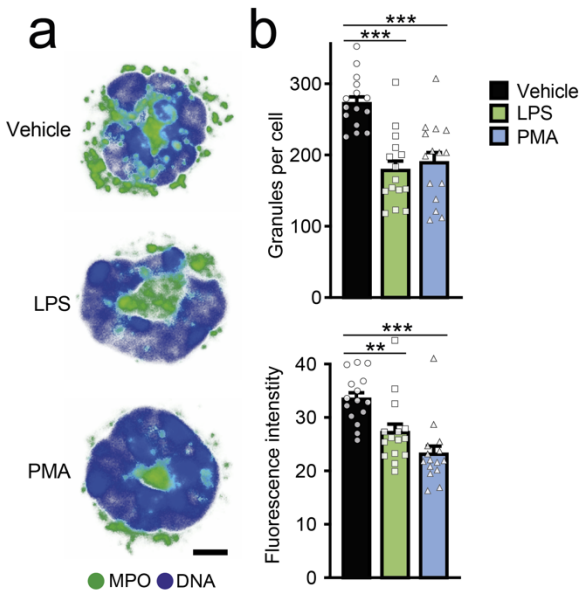

Extended Data Figure 3. CXCR2-deficient neutrophils are responsive to activating stimuli. **a**, Representative confocal images (scale, 2 μm) and **b**, quantification of granule content (top) and MPO intensity (bottom) in CXCR2-deficient neutrophils upon LPS or PMA stimulation. Granule loss indicates that CXCR2-deficient neutrophils are responsive to inflammatory stimuli; n = 15 cells per group. Data are shown as mean ± SEM. **; $p<0.01$; ***, $p<0.001$, as determined by one-way ANOVA with Dunnet's multiple comparison test.

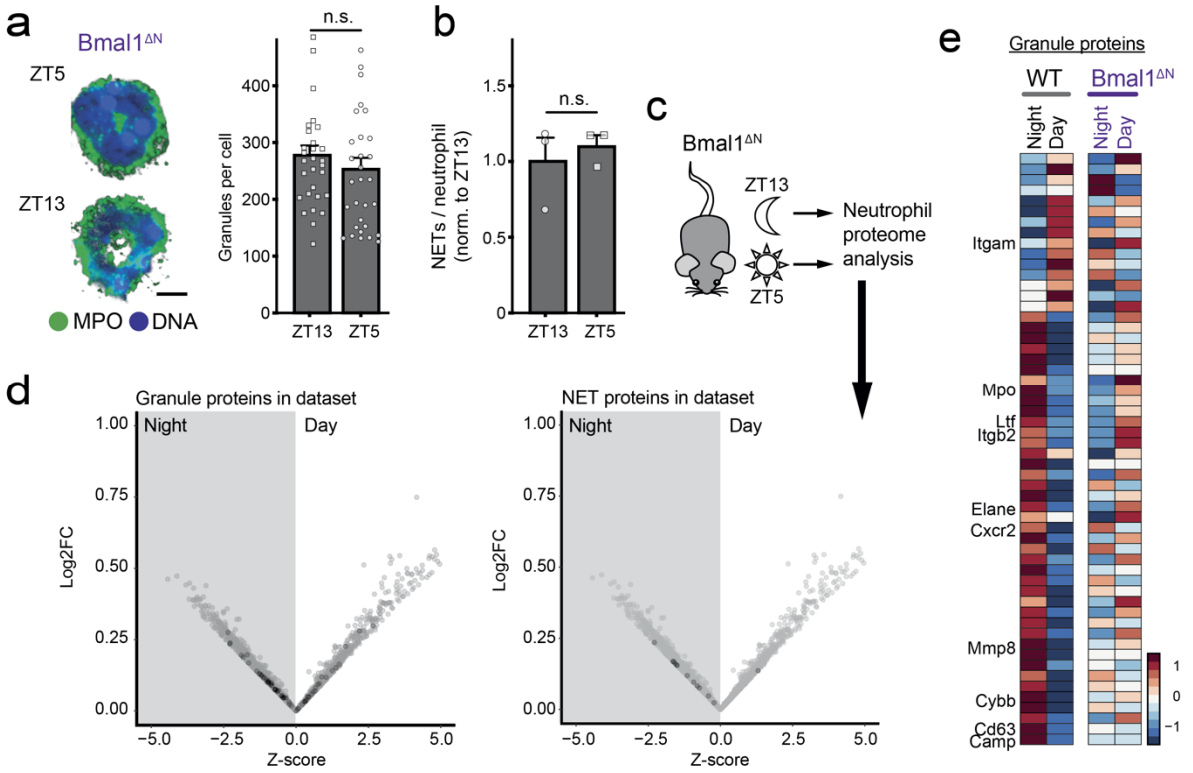

Extended Data Figure 4. Regulation of circadian patterns by Bmal1.

a, Representative confocal images (left) and quantification of granule content (right) in Bmal1-deficient neutrophils at ZT13 (night) and ZT5 (day). n = 30-31 cells from 3 mice; scale 2 μm. **b**, *Ex vivo* NET formation by Bmal1-deficient neutrophils at ZT5 and ZT13. Note that Bmal1-deficient neutrophils fail to display circadian oscillations in both granule and NET formation. n = 3 mice per time point. **c**, Experimental design of circadian proteomic analysis of Bmal1-deficient neutrophils. **d**, Granule proteins (left) and NET-associated proteins (right) in the circadian Bmal1$^{\Delta N}$ neutrophil proteome (n = 3 mice at ZT5 and n = 2 at ZT13). Black dots show all granule or NET-associated proteins, respectively, none of which reached significance in differential expression between night and day (FDR<0.05, see methods section for TMT proteomics of mouse neutrophils). **e**, Heatmap of granule proteins in the circadian proteome of wild-type (same as in **Figure 1**) and Bmal1$^{\Delta N}$ neutrophils. Note that the diurnal pattern is lost in Bmal1-deficient neutrophils. Data in (a-b) are shown as mean ± SEM; n.s., not significant, as determined by unpaired two-tailed t-test.

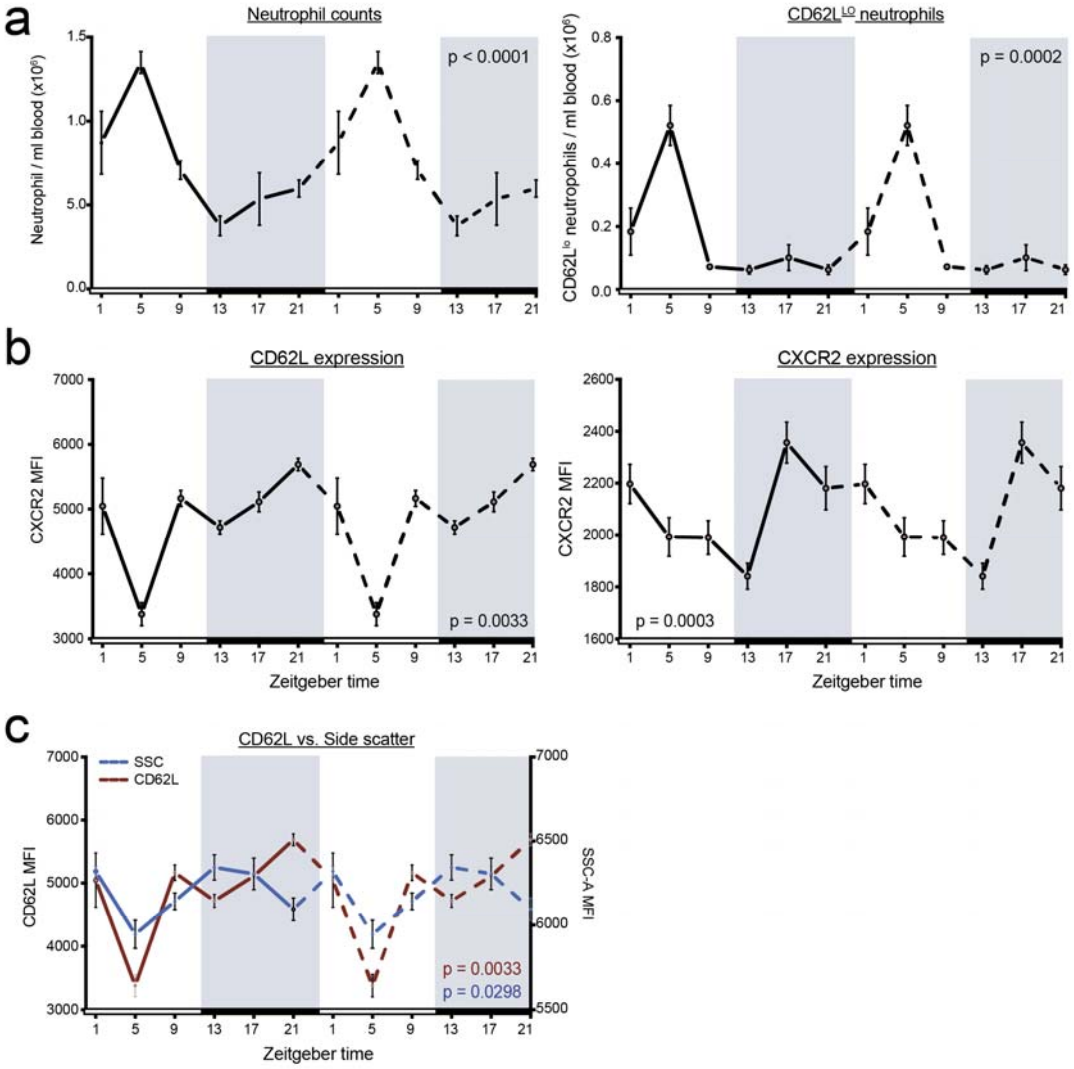

Extended Data Figure 5. Normal circadian oscillations in Balb/c mice.

a, Total (left) and CD62^{LO} aged (right) neutrophil counts in the blood of Balb/c mice; n = 4-5 mice per time. **b**, Circadian oscillations in CD62L and CXCR2 expression in neutrophils from Balb/c mice, measured as median fluorescence intensity (MFI) by flow cytometry n = 5 mice (ZT13, ZT17, ZT21, ZT1 and ZT9), n = 4 mice (ZT5). **c**, Side scatter values plotted together with surface levels of CD62L in neutrophils, showing similar fluctuation patterns as reported for C57BL/6 neutrophils; n = 5 mice (ZT13, ZT17, ZT21, ZT1 and ZT9), n = 4 mice (ZT5). All curves are repeated for two cycles (dashed line) to better appreciate the circadian pattern. Data are shown as mean ± SEM. P values were determined by the amplitude vs. zero two-tailed t-test.

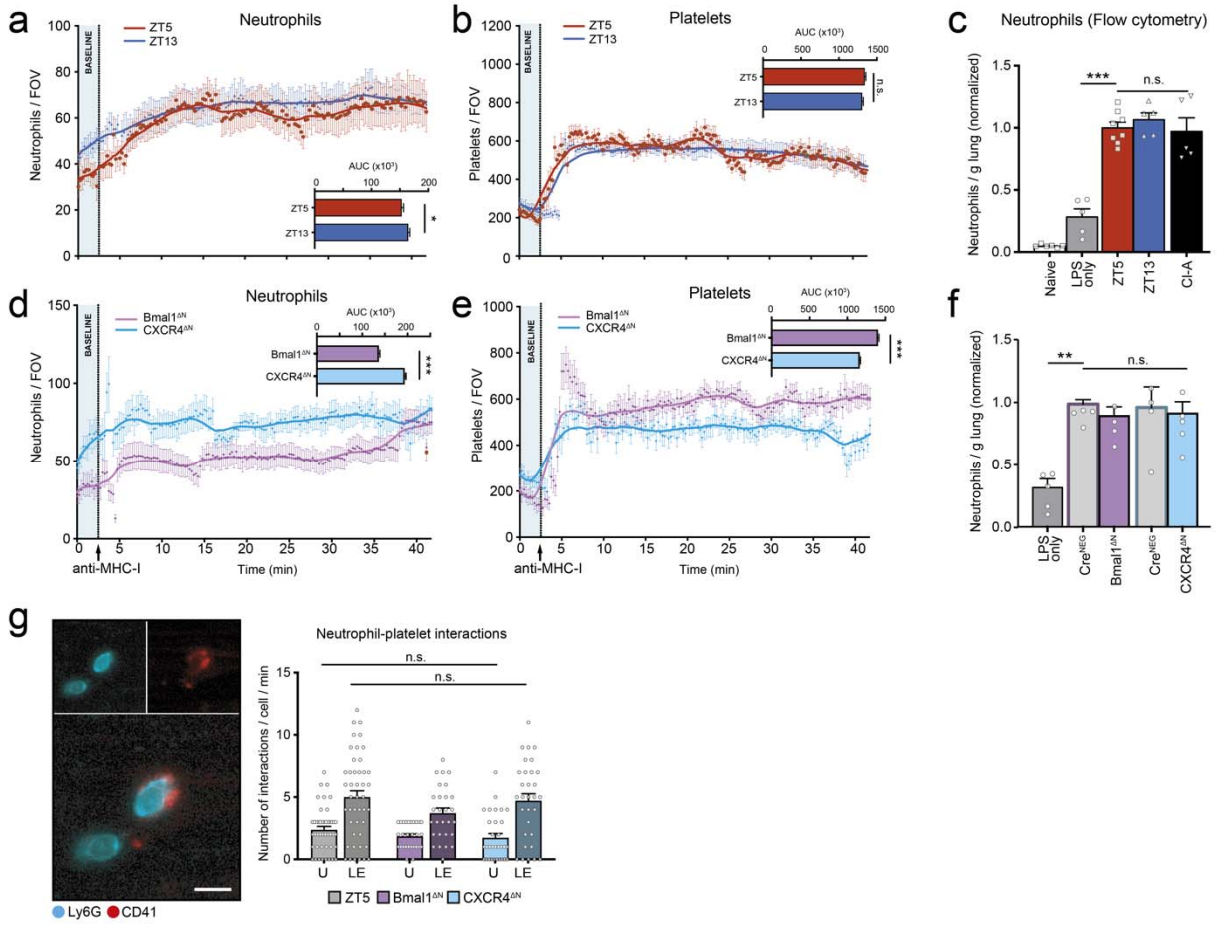

Extended Data Figure 6. Neutrophils and platelets in the lung microvasculature during ALI.

Quantification of neutrophil **a**, and platelet **b**, numbers per field of view over time in wild-type mice subject to ALI at night (ZT13, blue line) or during daytime (ZT5, red line), in the intravital imaging experiments shown in **Figure 4c**. Insets show area under the curve (AUC) values; n = 15 fields from 4 mice in each group. **c**, Neutrophil numbers in the lungs of naïve, LPS-only and wild-type mice in which ALI was induced at ZT5 (n = 8 mice) or ZT13 (n = 5 mice), or at ZT5 in the presence of Cl-amidine (n = 5 mice), as determined by flow cytometry. Neutrophils **d**, and platelets **e**, numbers in mutant mice (Bmal1$^{\Delta N}$ purple line; CXCR4$^{\Delta N}$ blue line) from the intravital imaging experiments shown in **Figure 5d**; n = 15 fields from 4 mice in each genotype. Insets show area under the curve (AUC) values. **f**, Neutrophil numbers in the lungs of LPS-only control mice (n = 5) or during ALI in Bmal1$^{\Delta N}$ (n = 4 mice) or Cre- control (n = 4 mice); and CXCR4$^{\Delta N}$ (n = 5 mice) or Cre- control mice (n = 4 mice), as determined by flow cytometry. **g**, Interactions between platelets and the uropod (U) or leading edge (LE) of adherent neutrophils, in the inflamed cremasteric microvessels of wild-type (n = 45 from 3 mice), Bmal1$^{\Delta N}$ (n = 28 from 3 mice) and CXCR4$^{\Delta N}$ mice (n = 31 from 3 mice); scale, 5 μm. Data are shown as mean ± SEM. **; p<0.01; ***, p<0.001; n.s., not significant, as determined by unpaired two-tailed t-test analysis (a-d) or one-way ANOVA with Dunnet's multiple comparison test (e-g). In the insets in a-d, individual data

points are not shown as this graph uses a mean ± SEM value for the area under the curve calculated from the data shown in the respective panels.

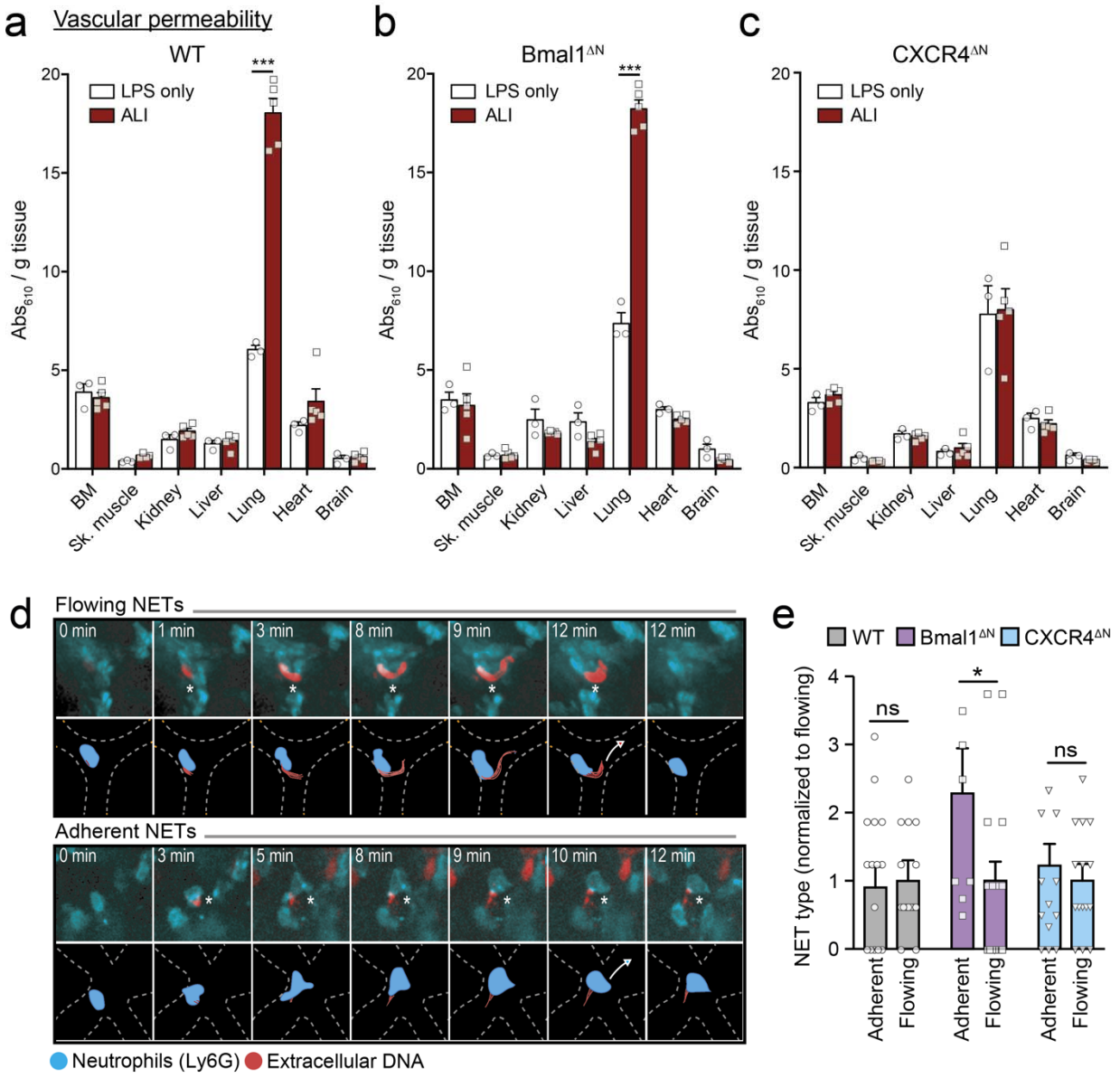

Extended Data Figure 7. Vascular leakiness and types of NETs during ALI.
Vascular leakiness in **a**, wild-type, **b**, Bmal1$^{\Delta N}$**,** and **c**, CXCR4$^{\Delta N}$ mice after induction of ALI (LPS + antibody) or in control mice treated with LPS only. WT and Bmal1$^{\Delta N}$ mice displayed increased leakiness only in lungs upon ALI induction, while CXCR4$^{\Delta N}$ mice were protected; n = 3 (LPS only) and 5 (ALI) mice per genotype; **d**, Time-lapse images showing examples of flowing and adherent NETs (asterisks) as observed by intravital imaging of the lung microvasculature during ALI, representative of n = 3 independent experiments. See also **Movie S5**. **e**, Relative frequency of NET types in WT, Bmal1$^{\Delta N}$ and CXCR4$^{\Delta N}$ mice during ALI, n = 15 fields from 3 mice (WT), 10 fields from 3 mice (Bmal1$^{\Delta N}$) and 15 fields from 3 mice (CXCR4$^{\Delta N}$). Data are shown as mean ± SEM. *; p<0.05; ***, p<0.001; n.s., not significant, as determined by two-way ANOVA (a-c; unless otherwise specified, comparisons did not reach significance; and e).

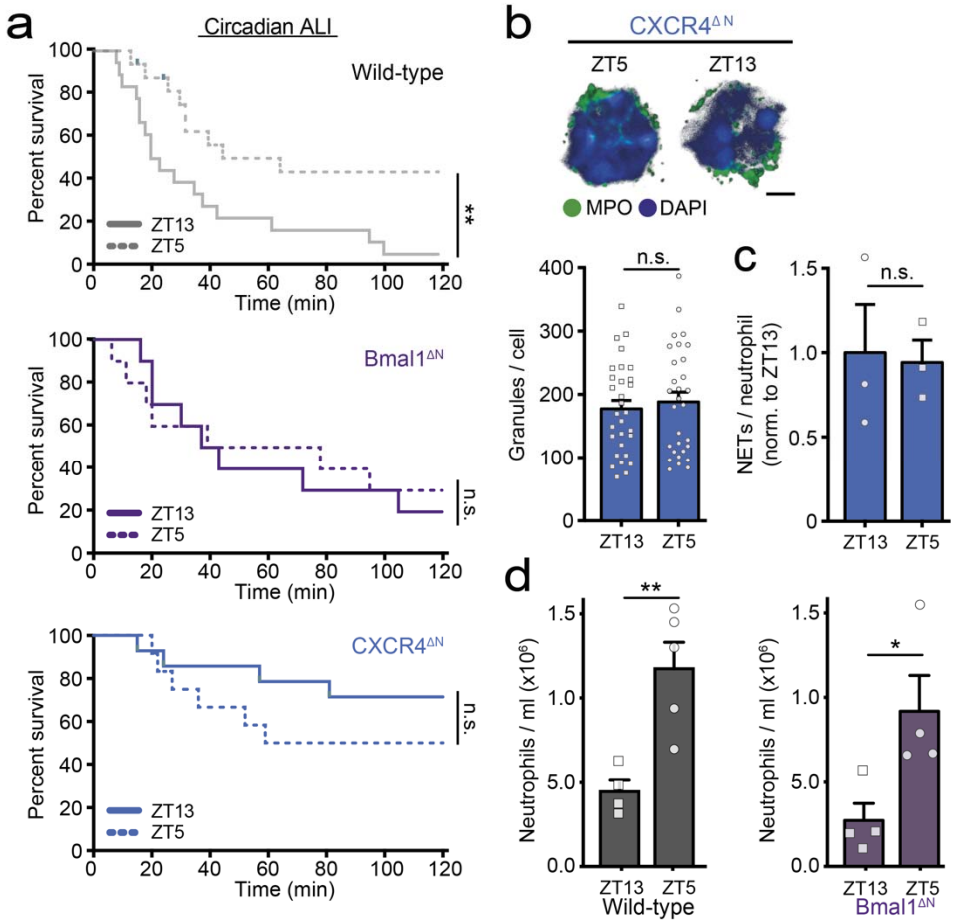

Extended Data Figure 8. Loss of circadian patterns in Bmal1$^{\Delta N}$ and CXCR4$^{\Delta N}$ mice.
a, Survival of wild-type, Bmal1$^{\Delta N}$ and CXCR4$^{\Delta N}$ mice subjected to ALI at night (ZT13, solid line) or daytime (ZT5, dashed line); n = 16 mice (ZT5) and 18 mice (ZT13) for wild-type, n = 10 mice per time point for Bmal1$^{\Delta N}$; n = 12 mice (ZT5) and 14 mice (ZT13) for CXCR4$^{\Delta N}$. **b**, Representative confocal images (top) and quantification of granule content (bottom) in CXCR4-deficient neutrophils at ZT13 and ZT5. Note the loss of diurnal fluctuations compared with wild-type mice (see **Figure 1e**); n = 30 cells (from 3 mice) per time point; scale, 2 μm. **c**, Ex vivo NET formation after PMA stimulation by CXCR4$^{\Delta N}$ neutrophils analyzed at ZT13 (n = 3 mice) and ZT5 (n = 3 mice). Note the loss of diurnal changes in NET-formation compared with wild-type cells (see **Figure 2b**); **d**, Neutrophil counts in blood at ZT5 and ZT13 in wild-type (n = 5 mice at ZT5 and 4 mice at ZT13) and Bmal1$^{\Delta N}$ mice (n = 4 mice per time point). Data are shown as mean ± SEM. *, p<0.05; **, p<0.01; n.s., not significant, as determined by two-sided log rank (Mantel-Cox) test (a) or unpaired two-tailed t-test (b-d).

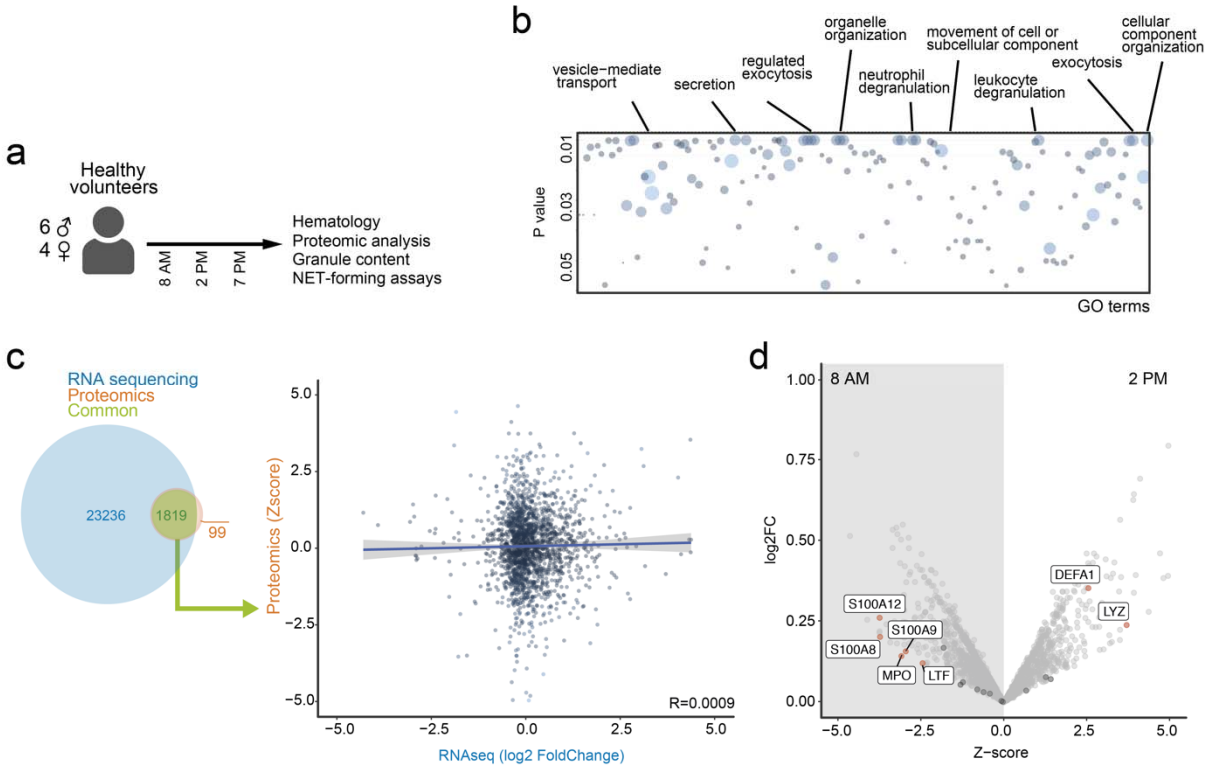

Extended Data Figure 9. Analysis of the human neutrophil proteome.
a, Experimental design. Blood from 10 healthy volunteers was extracted at 8 am, 2pm and 7 pm. Neutrophils were purified for proteomic analysis, granule quantification and NET-formation assays. **b**, GO terms of the differentially expressed proteins between 8am and 2pm in human neutrophils. **c**, Correlation analysis (Spearman) of the direction of change of common proteins and genes from paired human proteomic (n = 5 per time) and RNA sequencing (n = 3 per time) analysis, showing poor correlation of RNA and protein content. **d**, Volcano plot of the human neutrophil proteome highlighting proteins found in NETs. Red dots and labels show proteins that are significantly different among samples ($p < 0.05$), and black dots show all other NET proteins, and light-gray dots show the whole proteome dataset.

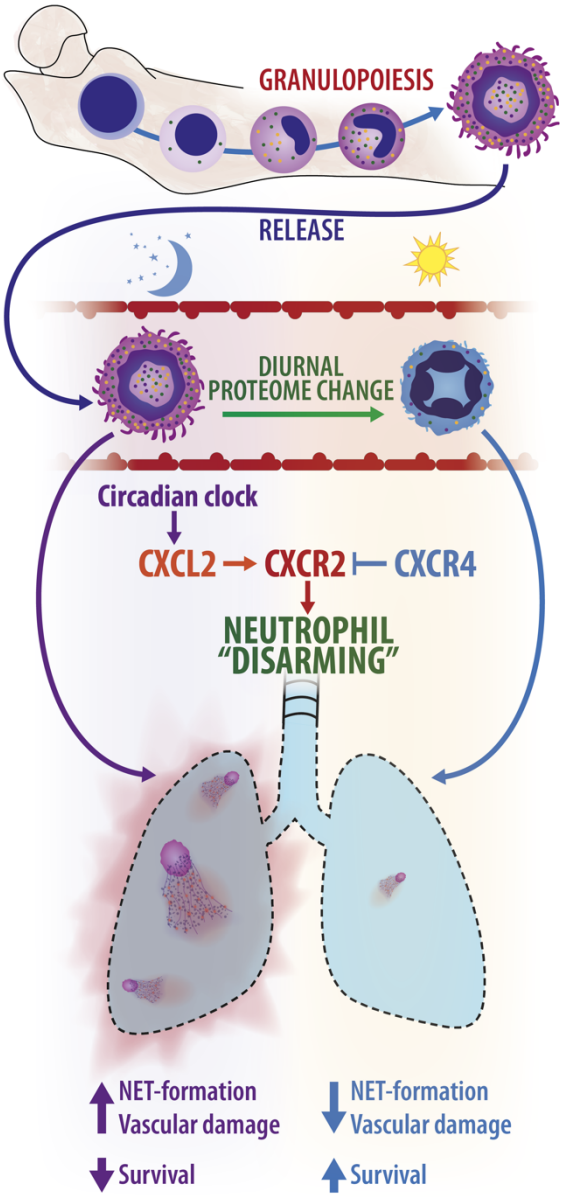

Extended Data Figure 10. Graphical abstract.
Neutrophils are released from the bone marrow into the bloodstream enriched in granule-held antimicrobial, cytotoxic and NET-forming proteins. As they spend time in the circulation, they undergo a homeostatic process of proteome "disarming" that is regulated by the clock gene Bmal1 and signaling through CXCR2. This process causes a reduction in granule content and their ability to form NETs, ultimately reducing their toxicity towards host tissues. During acute lung injury, the presence of granule-poor neutrophils at specific times of day or in CXCR4 mutants protects the lungs and increases survival. Disabling homeostatic degranulation in Bmal1 mutants, in contrast, increases organ damage and death at all times of day.

Legends for movies.

Movie S1.
Whole mount immunostaining of clarified lungs showing almost complete absence of NETs in naïve lungs before ALI induction. Lungs were stained for MPO (neutrophils), DNA, citrunillated-histone 3 and CD31. NETs were defined as triple-positive MPO-DNA-citH3 events. Representative of 3 independently cleared lungs.

Movie S2.
Whole mount immunostaining of clarified lungs during ALI, showing abundant NETs scattered throughout the lung. Lungs were stained for MPO (neutrophils), DNA, citrunillated-histone 3 and CD31. NETs were defined as triple-positive MPO-DNA-citH3 events. Representative of 3 independently cleared lungs.

Movie S3.
Intravital imaging of lungs during ALI, showing the formation of NET-like events in the pulmonary microvasculature. When ALI is induced at night (ZT13), more NET-like events (arrows) are produced compared with induction at noon (ZT5). Mice were treated intravenously with fluorescent anti-Ly6G to label neutrophils, and Sytox green for extracellular DNA. NET-like events are defined as those in which DNA is extruded from a neutrophil. Representative of 4 independent mice per time.

Movie S4.
3D reconstruction of CT scans of lungs from WT, Bmal1$^{\Delta N}$ and CXCR4$^{\Delta N}$ mice before (t = 0) and after acute lung injury induction (t = 21). The appearance of edema is shown by fluid accumulation (red) in the lungs, and bones are shown for reference. Representative of 7 independent mice per genotype.

Movie S5.
Intravital microscopy of the lung microcirculation showing the two identified types of NETs produced by neutrophils during ALI: Flowing NETs in which DNA is extruded out of the neutrophil body and is washed away by the blood flow; and adherent NETs, in which DNA is slowly extruded as the neutrophil crawls on the vessel, and adheres to the endothelial surface. Examples of both are shown. Representative of 9 independent experiments

Movie S6.
Video abstract. Neutrophils are released from the bone marrow into the bloodstream enriched in granule-held antimicrobial, cytotoxic and NET-forming proteins. As they spend time in the circulation, they undergo a homeostatic process of proteome “disarming” that is regulated by the clock gene Bmal1 and signaling through CXCR2. This process causes a reduction in granule content and their ability to form NETs, ultimately reducing their toxicity towards host tissues. During acute lung injury, the presence of granule-poor neutrophils at specific times of day or in CXCR4 mutants protects the lungs and increases survival. Disabling homeostatic degranulation in Bmal1 mutants, in contrast, increases organ damage and death at all times of day.

Legends for supplementary tables.

Table S1.
Proteomic data (related to Figure 1) of night-like and day-like neutrophils. Protein Id, identifier of each protein. Z, Z-score (positive values indicate increased representation in night neutrophils); FDR, false discovery rate. From single samples of 60 million neutrophils polled from 9 mice (night) and 6 mice (day). See methods for ^{18}O proteomics for details.

Table S2.
Full Gene Ontology (GO) Terms table, related to Supplementary Figure 1B and Table S1.

Table S3.
List of granule-held proteins and the granule type in which they are normally stored.

Table S4.
Proteomic data (related to Supplementary Figure 1D) of wild-type mouse neutrophils treated with AMD3100 (n = 3) or vehicle (n = 3) and sorted at ZT5. Protein Id, identifier of each protein. Columns 2-7: individual Z values. Integrated Z, integrated Z-score (positive values indicate increased representation in 8am neutrophils); FDR, false discovery rate. See methods for TMT proteomics of mouse neutrophils for details.

Table S5.
Proteomic data (related to Supplementary Figure 4D-E) of Bmal1$^{\Delta N}$ neutrophils at ZT13 (n = 2) and ZT5 (n = 3). Protein Id, identifier of each protein. Columns 2-6: individual Z values. Integrated Z, integrated Z-score (negative values indicate increased representation in night neutrophils); FDR, false discovery rate. See methods for TMT proteomics of mouse neutrophils for details.

Table S6.
Proteomic data (related to Figure 6) of human neutrophils at 8AM (n = 5) and 2PM (n = 5). Protein Id, identifier of each protein. Z, integrated Z-score (positive values indicate increased representation in 8am neutrophils); FDR, false discovery rate. See methods for TMT proteomics of human neutrophils for details.

Table S7.
Full Gene Ontology (GO) Terms table of the human proteomic data, related to Supplementary Figure 9B and Table S6.

Table S8.
Statistical parameters from the different quantitative proteomics experiments.